

Phenomenology of the simplest linear seesaw mechanism

Aditya Batra,^{1,2,*} Praveen Bharadwaj,^{1,†} Sanjoy
Mandal,^{3,‡} Rahul Srivastava,^{1,§} and José W. F. Valle^{4,¶}

¹*Department of Physics, Indian Institute of Science Education and Research - Bhopal,
Bhopal Bypass Road, Bhauri, Bhopal 462066, India*

²*Departamento de Física and CFTP, Instituto Superior Técnico,
Universidade de Lisboa, Av. Rovisco Pais 1, 1049-001 Lisboa, Portugal*

³*Korea Institute for Advanced Study, Seoul 02455, Korea*

⁴*AHEP Group, Institut de Física Corpuscular –
CSIC/Universitat de València, Parc Científic de Paterna.
C/ Catedrático José Beltrán, 2 E-46980 Paterna (Valencia) - SPAIN*

The linear seesaw mechanism provides a simple way to generate neutrino masses. In addition to Standard Model particles, it includes quasi-Dirac leptons as neutrino mass mediators, and a leptophilic scalar doublet seeding small neutrino masses. Here we review its associated physics, including restrictions from theory and phenomenology. The model yields potentially detectable $\mu \rightarrow e\gamma$ rates as well as distinctive signatures in the production and decay of heavy neutrinos (N_i) and the charged Higgs boson (H^\pm) arising from the second scalar doublet. We have found that production processes such as $e^+e^- \rightarrow NN$, $e^-\gamma \rightarrow NH^-$ and $e^+e^- \rightarrow H^+H^-$ followed by the decay chain $H^\pm \rightarrow \ell_i^\pm N$, $N \rightarrow \ell_j^\pm W^\mp$ leads to striking lepton number violation signatures at high energies which may probe the Majorana nature of neutrinos.

1. INTRODUCTION

Non-zero neutrino masses [1–4] constitute one of the most convincing proofs of new physics. Underpinning their ultimate origin stands out as one of the biggest challenges in elementary particle physics. Despite many attempts, the issue remains wide open. A simple way to generate Majorana neutrino masses is to introduce a non-renormalizable

*Electronic address: aditya.batra@tecnico.ulisboa.pt

†Electronic address: praveen20@iiserb.ac.in

‡Electronic address: smandal@kias.re.kr

§Electronic address: rahul@iiserb.ac.in

¶Electronic address: valle@ific.uv.es

dimension-five operator into the Standard Model (SM) [5]. The effective dimension-five operator characterizing lepton number non-conservation is given by

$$-\mathcal{L}_\nu^{d=5} = \frac{1}{\Lambda}(L\Phi)(\Phi L) + \text{H.c.}, \quad (1)$$

where the contractions involve the left-handed lepton doublet spinors L and the SM Higgs scalar doublet Φ . Here Λ is the effective mass scale, flavor indices are omitted, for brevity, and 2-dimensional conjugation matrices in Lorentz and isospin space are understood.

Neutrino mass model-building requires a completion of this operator. The seesaw mechanism provides a specially interesting one, and is most generally realized within the simplest $SU(3)_c \otimes SU(2)_L \otimes U(1)_Y$ gauge structure [6]. In its type-I realization, neutrinos get mass due to the exchange of heavy singlet fermion mediators. This leads to a Majorana mass for the left-handed neutrinos as $m_\nu \sim m_D^2/M_N$, with $m_D = Y_\nu v/\sqrt{2}$, so that $\Lambda = M_N/Y_\nu^2$. Hence, for $m_\nu \sim \mathcal{O}(0.1 \text{ eV})$ and a relatively large Yukawa coupling $Y_\nu \sim \mathcal{O}(1)$, M_N must be large, i.e., $M_N \gg \mathcal{O}(\text{TeV})$. As a result, the conventional high-scale implementation of the seesaw mechanism has few phenomenological implications other than those directly related to neutrino masses.

However, the seesaw paradigm can arise from low-scale physics. The low-scale seesaw varieties are the inverse [7, 8] and the linear seesaw mechanisms [9–11]. These share a common “(3,6)” template [6, 12]¹, which instead of a single right-handed neutrino, requires a sequential pair of isosinglet leptons associated to each family. The possibility that the heavy neutrinos could be produced at high energy colliders [13–19] was taken up by experiments, such as ATLAS and CMS at the LHC [20–22] and also future proposals [23–25].

Interestingly enough, leptonic flavour and CP can be violated even in the limit of massless neutrinos [26–29]. This implies that such processes need not be suppressed by the small neutrino masses, and can in fact have observable rates [26, 27, 29–32]². Detailed charged lepton flavour violation (cLFV) predictions depend on whether one has an inverse or linear seesaw realization, and also on details of Yukawa coupling matrices [37].

In this work, we examine the simplest SM-based variant of the linear seesaw mechanism. In contrast to most previous formulations [9–11], here we do not impose left-right symmetry. The linear seesaw mechanism is realized within the $SU(3)_c \otimes SU(2)_L \otimes U(1)_Y$ gauge structure itself, in which lepton number symmetry is ungauged [38]. We assume at least two pairs of isosinglet leptons. In addition, the scalar sector contains a second Higgs doublet, carrying two units of lepton number.

Even for TeV-scale mediators, $M_N \sim \mathcal{O}(\text{TeV})$, neutrino masses are naturally small due to

¹ These contain 6 singlets that make up 3 heavy Dirac leptons in the limit of lepton number conservation.

² For generic references on cLFV in seesaw schemes see, for example [33–36].

the small vacuum expectation value (VEV) of this second Higgs doublet. For simplicity, we assume that lepton number symmetry is broken explicitly, but softly, in the scalar potential, thereby avoiding a Nambu-Goldstone boson and the associated stringent astrophysical restrictions [38]. Such a “neutrino-motivated” version of the two-doublet model [39–41] allows for direct experimental tests [42], as we will discuss later. The charged scalar also contribute to lepton flavor violating decays such as, $\mu \rightarrow e\gamma$, with rates that can lie within reach of current experiment [43], providing extra sensitivity to model parameters.

Note that our pair production of charged scalars at e^+e^- collider is in sharp contrast with the usual two Higgs doublet model (THDM), in which it proceeds via the neutral current Drell-Yan mechanism involving s-channel γ/Z exchange. In our linear seesaw scheme the pair production of charged scalars at e^+e^- collider can be dominated by a t-channel heavy-neutrino-mediated diagram. The decays of the new scalars are controlled by the underlying $U(1)$ lepton symmetry and we find that when the charged Higgs mass $m_{H^\pm} > M_{N_i}$, the decay chain $H^\pm \rightarrow \ell^\pm N_i, N_i \rightarrow \ell_j^\pm W^\mp$ leads to striking signatures. Our proposal also leads to new production mechanisms for heavy neutrinos involving t-channel charged Higgs mediation, $e^+e^- \rightarrow N_i N_i$ and associated production through $e^- \gamma \rightarrow N_i H^-$. In contrast to other type-I seesaw schemes, in our linear seesaw model $e^+e^- \rightarrow N_i N_i$ production is not suppressed by light-heavy neutrino mixing.

The paper is organized as follows. To make our presentation self-contained, in Sec. 2 we briefly recap the model, giving details of its new fields and their interactions. In Sec. 3, we discuss constraint from electroweak precision parameters S , T and U . In Sec. 5, we discuss the existing collider constraints on the new scalar masses. In Sec. 4, we discuss various phenomenological implications for charged lepton flavour violation processes. In Sec. 6 and 7, we discuss various possible production mechanisms at e^+e^- [23, 44–46], $e^- \gamma$ [47–52] colliders, and also various decay channels of heavy neutrinos and new scalars. In Sec. 8 we show how our linear seesaw model can lead to promising signatures at future lepton colliders, such as the ILC [44], FCC-ee [23], CLIC [45], and the CEPC [46]. Finally, in Sec. 9 we conclude.

2. LINEAR SEESAW MODEL

The linear seesaw is a low-scale variant of the seesaw mechanism first proposed within the $SU(3) \otimes SU(2)_L \otimes SU(2)_R \otimes U(1)_{B-L}$ gauge group [9, 10], and subsequently shown to arise also within the $SO(10)$ framework [11].

In this work, we propose the simplest variant of the linear seesaw mechanism, realized within the simplest $SU(3)_c \otimes SU(2)_L \otimes U(1)_Y$ gauge structure itself. Particle content and their representations under the SM gauge and global $U(1)_L$ lepton number symmetry are given in Table. I. Here, in addition to the SM Higgs scalar Φ , we add one more doublet χ_L ,

	Q	u^c	d^c	L	e^c	ν^c	S	Φ	χ_L
$SU(3)_C$	$\mathbf{3}$	$\mathbf{3}^*$	$\mathbf{3}^*$	$\mathbf{1}$	$\mathbf{1}$	$\mathbf{1}$	$\mathbf{1}$	$\mathbf{1}$	$\mathbf{1}$
$SU(2)_L$	$\mathbf{2}$	$\mathbf{1}$	$\mathbf{1}$	$\mathbf{2}$	$\mathbf{1}$	$\mathbf{1}$	$\mathbf{1}$	$\mathbf{2}$	$\mathbf{2}$
$U(1)_Y$	$\frac{1}{6}$	$-\frac{2}{3}$	$\frac{1}{3}$	$-\frac{1}{2}$	1	0	0	$\frac{1}{2}$	$\frac{1}{2}$
$U(1)_L$	0	0	0	1	-1	-1	1	0	-2

TABLE I: Linear-seesaw particle content and transformation properties under the SM gauge and global $U(1)_L$ lepton number symmetry. The subscript “L” in χ_L denotes its non-zero charge under the $U(1)_L$ symmetry.

carrying lepton number $L[\chi_L] = -2$ in order to seed neutrino mass generation. In contrast with Ref. [38] we do not add a gauge singlet scalar to implement the spontaneous breaking of the lepton number symmetry. The assumed breaking is explicit, thus avoiding the existence of a physical (nearly) massless Nambu-Goldstone boson, and the associated restrictions from LEP [53] as well as the stringent astrophysical limits from stellar cooling [38]. In addition to the new scalar doublet we add three lepton singlets ν_i^c with lepton number $L[\nu_i^c] = -1$ and three lepton singlets S_i with lepton number $L[S_i] = 1$. The global $U(1)$ lepton number symmetry is broken only in the scalar sector, explicitly but softly.

2.1. Neutrino mass generation

Here we focus on the simplest linear seesaw setup, a very simple extension of the Standard Model. In its simplest form the relevant lepton-number-invariant Lagrangian for neutrino mass generation is written as

$$-\mathcal{L}_{\text{Yuk}} = Y_\nu^{ij} L_i^T C \nu_j^c \Phi + M_R^{ij} \nu_i^c C S_j + Y_S^{ij} L_i^T C S_j \chi_L + \text{h.c.} \quad (2)$$

where Y_ν and Y_S are dimensionless Yukawa couplings, M_R is an arbitrary bare mass term, Φ is the SM Higgs doublet, while χ_L is the other scalar doublet. This form gives an effective description of more complete realizations with spontaneous breaking of gauged [9–11] or global lepton number [38].

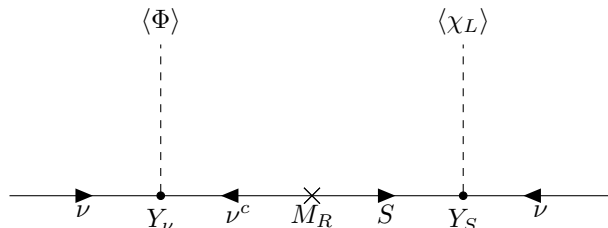


FIG. 1: Neutrino mass generation in the linear seesaw mechanism.

In the basis ν, ν^c, S the resulting linear seesaw mass matrix obtained after lepton number violation is

$$\mathcal{M}_\nu = \begin{pmatrix} 0 & m_D & M_L \\ m_D^T & 0 & M_R \\ M_L^T & M_R^T & 0 \end{pmatrix}. \quad (3)$$

The mass entry M_L is proportional to the VEV v_χ driving lepton number violation,

$$M_L = \frac{Y_S^{ij} v_\chi}{\sqrt{2}}, \quad (4)$$

while the other one is the conventional Dirac mass entry

$$m_D = \frac{Y_\nu^{ij} v_\Phi}{\sqrt{2}}, \quad (5)$$

given in terms of the SM Higgs VEV v_Φ . In order to generate VEV for χ_L , we break the global $U(1)_L$ lepton symmetry explicitly in the scalar sector using the soft term $\mu_{12}^2(\Phi^\dagger \chi_L + h.c.)$. This gives the following induced VEV for χ_L ,

$$v_\chi \approx \frac{\mu_{12}^2 v_\Phi}{m_A^2}, \quad (6)$$

where m_A is the mass of pseudoscalar which we define later. The full 9×9 neutrino mass matrix in Eq. (3) can be diagonalized by a unitary matrix $\mathcal{U}^\dagger \mathcal{M}_\nu \mathcal{U}^* = \mathcal{M}_\nu^{\text{diag}}$. Here \mathcal{U} is a product of a block-diagonalization followed by separate diagonalizations in the light and heavy sectors [12]. The matrix \mathcal{U} can be expressed as [12]

$$\mathcal{U} = \mathcal{U}_0 \mathcal{U}_1 \quad \text{with} \quad \mathcal{U}_0^\dagger \mathcal{M}_\nu \mathcal{U}_0^* = \begin{pmatrix} m_{\text{light}} & 0 \\ 0 & M_{\text{heavy}} \end{pmatrix}. \quad (7)$$

Hence, \mathcal{U}_0 first brings the full neutrino matrix to block diagonal form, while $\mathcal{U}_1 = \text{Diag}(\mathcal{U}_{\text{lep}}, \mathcal{U}_R)$ diagonalizes the mass matrices m_{light} and M_{heavy} . This matrix \mathcal{U} is expressed approximately as follows

$$\mathcal{U} \approx \begin{pmatrix} (1 - \frac{1}{2}\epsilon)U_{\text{lep}} & -\frac{i}{\sqrt{2}}V & \frac{1}{\sqrt{2}}V \\ 0 & \frac{i}{\sqrt{2}}(1 - \frac{1}{2}\epsilon') & \frac{1}{\sqrt{2}}(1 - \frac{1}{2}\epsilon') \\ -V^\dagger & -\frac{i}{\sqrt{2}}(1 - \frac{1}{2}\epsilon') & \frac{1}{\sqrt{2}}(1 - \frac{1}{2}\epsilon') \end{pmatrix}, \quad (8)$$

where V is a 3×3 matrix

$$V = m_D (M_R^T)^{-1}. \quad (9)$$

The parameters ϵ and ϵ' denote non-unitary corrections. Their explicit form is given as

$$\epsilon \approx (m_D M_R^{-1T})(M_R^{-1} m_D^\dagger) + \mathcal{O}(M_L^2/M_R^2), \quad (10)$$

$$\epsilon' \approx (M_R^{-1} m_D^\dagger)(m_D M_R^{-1T}) + \mathcal{O}(M_L^2/M_R^2). \quad (11)$$

The hierarchy $M_R \gg m_D \gg M_L$ implies an effective light neutrino mass matrix given as

$$m_{\text{light}} = m_D (M_L M_R^{-1})^T + (M_L M_R^{-1}) m_D^T. \quad (12)$$

The limit $M_L \rightarrow 0$ leads to three massless neutrinos as in the Standard Model, plus three heavy Dirac neutrinos, N . Approximate analytical forms for the charged and neutral current weak interaction matrices in this limit are given in [26, 28–30]. The above form provides the template for the low-scale seesaw schemes, including the inverse [7, 8] and the linear seesaw mechanisms [9–11]. After lepton number violation, a non-zero M_L is generated, leading to three light Majorana eigenstates ν_i , with $i = 1, 2, 3$ and six heavy neutrinos $N_j, j = 4, \dots, 9$ which form three pairs of quasi-Dirac states [54, 55]. The neutrino mass generation mechanism is illustrated by the Feynman diagram shown in Fig. 1. One sees that, in contrast to the conventional type-I seesaw setups, the matrix m_{light} scales linearly with the Dirac Yukawa couplings contained in m_D , thus the name linear seesaw mechanism. Note that neutrino masses will be suppressed by the small value of M_L irrespective of how low the M_R scale characterizing the heavy messengers is, also allowing for non-negligible Y_S values. This is achieved with a very small value of v_χ . In the limit $\mu_{12} \rightarrow 0$ and hence $v_\chi \rightarrow 0$, lepton number is restored, so the construction is natural in t'Hooft's sense.

For completeness we also specify the charged-lepton and quark Yukawa Lagrangian terms,

$$-\mathcal{L}_{\text{Yuk}} = Y_e \bar{L}_L \Phi e_R + Y_u \bar{Q}_L \tilde{\Phi} u_R + Y_d \bar{Q}_L \Phi d_R + \text{h.c.} \quad (13)$$

Notice that, due to the $U(1)_L$ lepton number symmetry, charged fermions acquire mass only through their Yukawa coupling with the SM Higgs doublet Φ . Hence, the doublet χ_L is leptophilic. In this sense, as far as quarks are concerned, our simplest linear seesaw scheme resembles the Type I two-Higgs-doublet-Model (THDM) [39]. It follows that the Higgs Yukawa Lagrangian can be written compactly as

$$-\mathcal{L}_{\text{Yuk}} = \frac{m_f}{v \sin \beta} \bar{\psi}_f \psi_f (\cos \alpha h + \sin \alpha H), \quad (14)$$

for all charged fermions.

2.2. The scalar sector

In addition to the SM Higgs doublet Φ we also have a second scalar doublet χ_L , charged under lepton number. The $SU(3)_c \otimes SU(2)_L \otimes U(1)_Y$ gauge invariant scalar potential is given by

$$V = -\mu_\Phi^2 \Phi^\dagger \Phi - \mu_\chi^2 \chi_L^\dagger \chi_L + \lambda_1 (\Phi^\dagger \Phi)^2 + \lambda_2 (\chi_L^\dagger \chi_L)^2 + \lambda_3 \chi_L^\dagger \chi_L \Phi^\dagger \Phi + \lambda_4 \chi_L^\dagger \Phi \Phi^\dagger \chi_L - (\mu_{12}^2 \Phi^\dagger \chi_L + \text{H.c.}), \quad (15)$$

For definiteness, we assume all parameters to be real. In addition to breaking the electroweak gauge symmetry through the Higgs mechanism, this potential also breaks lepton number. We choose to do this explicitly, but “softly”, through the last bilinear term $\mu_{12}^2 (\Phi^\dagger \chi_L + \text{h.c.})$, which induces a non-zero VEV for χ_L .

We now examine the consistency conditions of the potential. To ensure that the scalar potential is bounded from below and has a stable vacuum at any given energy scale, the following constraints must hold:

$$\lambda_1 \geq 0, \quad \lambda_2 \geq 0, \quad \lambda_3 \geq -2\sqrt{\lambda_1 \lambda_2} \quad \text{and} \quad \lambda_3 + \lambda_4 \geq -2\sqrt{\lambda_1 \lambda_2}. \quad (16)$$

To ensure perturbativity, we also restrict the scalar quartic couplings in Eq. 15 to the range $\lambda_i \leq 4\pi$.

Higgs boson mass spectrum

After $SU(3)_c \otimes SU(2)_L \otimes U(1)_Y$ and lepton-number symmetry breaking, we obtain the mass spectrum for the scalars by expanding the scalar fields Φ and χ_L as

$$\Phi = \begin{pmatrix} \Phi^+ \\ \frac{1}{\sqrt{2}}(v_\Phi + h_\Phi + i\eta_\Phi) \end{pmatrix}, \quad \chi_L = \begin{pmatrix} \chi^+ \\ \frac{1}{\sqrt{2}}(v_\chi + h_\chi + i\eta_\chi) \end{pmatrix}, \quad (17)$$

where h_Φ , h_χ and η_Φ , η_χ are CP even and CP odd neutral scalars, while χ^\pm and Φ^\pm are charged scalars. In order to get the physical states and describe the mixing between the two doublets Φ and χ_L , we diagonalize the charged and neutral scalar mass matrix.

In addition to the three unphysical Goldstone bosons G^\pm, G^0 which are “eaten” to become the longitudinal components of the SM W^\pm and Z gauge bosons, there is one physical charged scalar H^\pm and three neutral scalars h, H, A , making up the eight degrees of freedom of the two-doublet-Higgs boson system.

The mass matrix for the charged scalars in the basis (χ^+, Φ^+) is given by

$$\mathcal{M}_\chi^2 = \begin{pmatrix} \mu_{12}^2 \frac{v_\Phi}{v_\chi} - \lambda_4 \frac{v_\Phi^2}{2} & -\mu_{12}^2 + \lambda_4 \frac{v_\Phi v_\chi}{2} \\ -\mu_{12}^2 + \lambda_4 \frac{v_\Phi v_\chi}{2} & \mu_{12}^2 \frac{v_\chi}{v_\Phi} - \lambda_4 \frac{v_\chi^2}{2} \end{pmatrix}. \quad (18)$$

This matrix has a zero eigenvalue corresponding to the charged Goldstone boson G^+ , so the physical charged Higgs has a mass

$$m_{H^\pm}^2 = v^2 \left(\frac{\mu_{12}^2}{v_\Phi v_\chi} - \frac{\lambda_4}{2} \right), \quad (19)$$

where $v = \sqrt{v_\Phi^2 + v_\chi^2}$. The charged mass-eigenstates are obtained as

$$\begin{pmatrix} \chi^+ \\ \Phi^+ \end{pmatrix} = R(\beta) \begin{pmatrix} G^+ \\ H^+ \end{pmatrix} = \begin{pmatrix} \cos \beta & -\sin \beta \\ \sin \beta & \cos \beta \end{pmatrix} \begin{pmatrix} G^+ \\ H^+ \end{pmatrix}, \quad \text{with } \tan \beta = \frac{v_\Phi}{v_\chi}. \quad (20)$$

Here, in defining the parameter $\tan \beta$, we have followed the Two-Higgs-Doublet-Model (2HDM) convention. However, in contrast to standard 2HDM models, where $\tan \beta$ is usually constrained by perturbativity of Yukawa couplings, in our case $\tan \beta$ can be naturally very large approaching $\tan \beta \rightarrow \infty$ as $v_\chi \rightarrow 0$.

The mass matrix for CP even neutral scalars in the basis (h_χ, h_Φ) is given as

$$\mathcal{M}_h^2 = \begin{pmatrix} A & C \\ C & B \end{pmatrix} = \begin{pmatrix} \mu_{12}^2 \frac{v_\Phi}{v_\chi} + 2\lambda_2 v_\chi^2 & -\mu_{12}^2 + v_\Phi v_\chi \lambda_{34} \\ -\mu_{12}^2 + v_\Phi v_\chi \lambda_{34} & \mu_{12}^2 \frac{v_\chi}{v_\Phi} + 2\lambda_1 v_\Phi^2 \end{pmatrix}, \quad (21)$$

where we defined $\lambda_{34} \equiv \lambda_3 + \lambda_4$. The masses of light and heavy eigenstates are given as

$$m_h^2 = \frac{1}{2}[A + B - \sqrt{(A - B)^2 + 4C^2}], \quad (22)$$

$$m_H^2 = \frac{1}{2}[A + B + \sqrt{(A - B)^2 + 4C^2}]. \quad (23)$$

The lighter mass eigenstate h is identified as the SM Higgs boson discovered at the LHC [56, 57]. Again following the 2HDM convention, the two mass eigenstates h and H are related with the h_χ, h_Φ fields through the rotation matrix $R(\alpha)$ as,

$$\begin{pmatrix} h_\chi \\ h_\Phi \end{pmatrix} = R(\alpha) \begin{pmatrix} H \\ h \end{pmatrix} = \begin{pmatrix} \cos \alpha & -\sin \alpha \\ \sin \alpha & \cos \alpha \end{pmatrix} \begin{pmatrix} H \\ h \end{pmatrix}, \quad \text{with } \tan 2\alpha = \frac{2C}{A - B}. \quad (24)$$

The pseudoscalar mass matrix in the basis (η_χ, η_Φ) is given by

$$\mathcal{M}_\eta^2 = \begin{pmatrix} \mu_{12}^2 \frac{v_\Phi}{v_\chi} & -\mu_{12}^2 \\ -\mu_{12}^2 & \mu_{12}^2 \frac{v_\chi}{v_\Phi} \end{pmatrix}. \quad (25)$$

One sees that this pseudoscalar mass matrix has a zero-mass eigenvalue, corresponding to the Goldstone boson G^0 eaten by the Z , while the physical pseudoscalar Higgs has a mass

$$m_A^2 = \mu_{12}^2 \frac{v^2}{v_\Phi v_\chi}. \quad (26)$$

The mass eigenstates are again obtained by rotating the component fields as

$$\begin{pmatrix} \eta_\chi \\ \eta_\Phi \end{pmatrix} = R(\beta) \begin{pmatrix} G^0 \\ A \end{pmatrix} = \begin{pmatrix} \cos \beta & -\sin \beta \\ \sin \beta & \cos \beta \end{pmatrix} \begin{pmatrix} G^0 \\ A \end{pmatrix} \quad \text{with} \quad \tan \beta = \frac{v_\Phi}{v_\chi}. \quad (27)$$

From Eq. 26 the pseudoscalar mass is proportional to μ_{12} , which comes from the explicit lepton number soft breaking term $\mu_{12}^2 \Phi^\dagger \chi_L$. Should this term not be present in the potential, this pseudoscalar would be an unwanted doublet “majoron”, ruled out by the measurements of the invisible decay width of the Z boson at LEP [53, 58]. Such a “majoron” would also be copiously produced in stars, leading to an astrophysical disaster. The most straightforward way to avoid this is to give it a mass, through Eq. 26.

An alternative possibility to implement the spontaneous breaking of lepton number symmetry would be to “invisibilize” the majoron by adding another singlet scalar carrying lepton number. This possibility has already been examined and we refer the interested reader to [38].

As we assume explicit lepton number violation, the Higgs potential is the minimal one. One can describe all its quartic couplings in terms of the just four physical masses, m_h, m_H, m_A and m_{H^\pm} , and the angles β and α . Indeed, the quartic couplings $\lambda_1, \lambda_2, \lambda_3$ and λ_4 can be expressed as

$$\lambda_1 = \frac{1}{2v^2 \sin^2 \beta} \left(m_H^2 \sin^2 \alpha + m_h^2 \cos^2 \alpha - m_A^2 \cos^2 \beta \right), \quad (28)$$

$$\lambda_2 = \frac{1}{2v^2 \cos^2 \beta} \left(m_h^2 \sin^2 \alpha + m_H^2 \cos^2 \alpha - m_A^2 \sin^2 \beta \right), \quad (29)$$

$$\lambda_3 = \frac{1}{v^2} \left(2m_{H^\pm}^2 - m_A^2 + \frac{(m_H^2 - m_h^2) \sin(2\alpha)}{\sin(2\beta)} \right), \quad (30)$$

$$\lambda_4 = \frac{2}{v^2} \left(m_A^2 - m_{H^\pm}^2 \right), \quad (31)$$

where the VEV $v = 246$ GeV. Note that since $v^2 \sin^2 \beta = v_\Phi^2$ and $v^2 \cos^2 \beta = v_\chi^2$, the quartic

couplings $\lambda_1 \propto \frac{1}{v_\Phi^2}$ whereas $\lambda_2 \propto \frac{1}{v_\chi^2}$. This has important implications for the mass spectrum of the scalars as we discuss next.

Compressed spectrum

As we saw in Eq. 4, the smallness of neutrino mass requires a very small value of the lepton number breaking scale v_χ but allows us to have a relatively large Yukawa coupling Y_S . We note that scalar spectrum tends to be very compressed when v_χ is small. This is required in order for λ_2 to be in the perturbative regime, as can be seen from the expression of λ_2 in Eq. 29. Indeed, as λ_2 is inversely proportional to v_χ^2 and, for tiny v_χ , a small numerator is achieved when $m_H \approx m_A$ and $\alpha \approx 0$. The left panel of Fig. 2 shows the splitting $|m_H - m_A|$ with respect to v_χ . One clearly sees that the splitting $|m_H - m_A|$ is very small as long as v_χ is small.

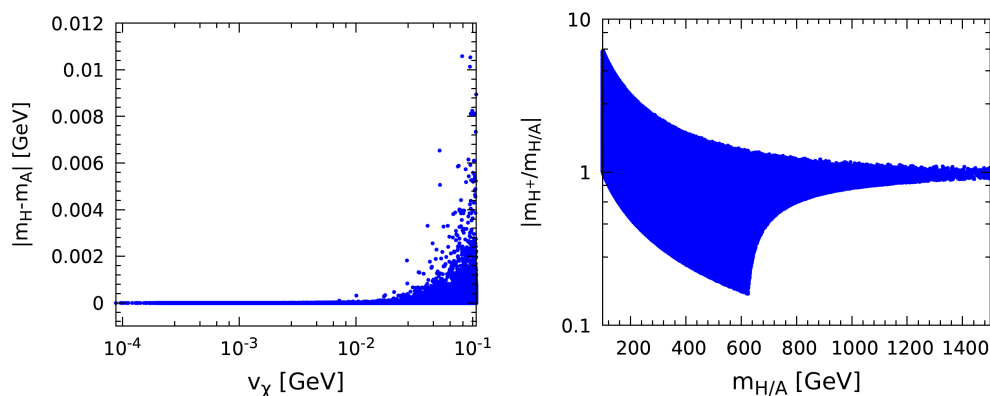


FIG. 2: Left panel: $|m_H - m_A|$ versus the lepton number breaking scale v_χ . Right panel: $|m_{H^\pm}/m_{H/A}|$ versus $m_{H/A}$, for $v_\chi < 10^{-1}$ GeV, so that $\alpha \approx 0$ and $m_H \approx m_A$.

In the limit $\alpha \approx 0$, $m_H \approx m_A$ and $v_\chi \ll v_\Phi$, the quartic couplings λ_3 , λ_4 simplify to $\lambda_3 \approx (2m_{H^\pm}^2 - m_A^2)/v^2$, $\lambda_4 \approx 2(m_A^2 - m_{H^\pm}^2)/v^2$. This suggests that the mass-splitting between m_{H^\pm} and $m_{H/A}$ must be restricted in order to keep λ_3 , λ_4 within the perturbative regime. This is shown in the right panel of Fig. 2 where we have plotted the ratio $|m_{H^\pm}/m_{H/A}|$ with respect to $m_{H/A}$. One sees that H^\pm and H/A can be non-degenerate in mass when $m_{H/A}$ is relatively small. However, for $m_{H/A} > 1$ TeV, all scalars, H^\pm and H/A , become very degenerate in mass. Note that all of this changes if v_χ is relatively large. In such a case, the mixing angle α can be large, and the mass degeneracy between H , A , and H^\pm can be lifted.

3. ELECTROWEAK PRECISION PARAMETERS S , T AND U

The presence of the extra doublet χ_L in the linear seesaw model modifies the prediction for different radiative corrections, especially the oblique parameters S , T , U [59]. The general

form of these are given in Ref. [60]. For the case of small v_χ , the oblique parameters S , T and U take the following simple form:

$$T \approx \frac{1}{8\pi s_W^2 m_W^2} F(m_{H^\pm}^2, m_H^2), \quad S \approx \frac{1}{12\pi} \log \left(\frac{m_H^2}{m_{H^\pm}^2} \right), \quad U \approx \frac{1}{12\pi} G\left(\frac{m_{H^\pm}^2}{m_W^2}, \frac{m_H^2}{m_W^2}\right), \quad (32)$$

where the functions F and G are as shown in Ref. [60]:

$$F(x, y) = \begin{cases} \frac{x+y}{2} - \frac{xy}{x-y} \ln \frac{x}{y} & \Leftarrow x \neq y, \\ 0 & \Leftarrow x = y. \end{cases} \quad (33)$$

$$G(x, y) = -\frac{16}{3} + 5(x+y) - 2(x-y)^2 + 3 \left[\frac{x^2+y^2}{x-y} - x^2 + y^2 + \frac{(x-y)^3}{3} \right] \ln \frac{x}{y} \quad (34)$$

$$+ [1 - 2(x+y) + (x-y)^2] f(x+y-1, 1 - 2(x+y) + (x-y)^2),$$

where

$$f(z, w) = \begin{cases} \sqrt{w} \ln \left| \frac{z - \sqrt{w}}{z + \sqrt{w}} \right| & \Leftarrow w > 0, \\ 0 & \Leftarrow w = 0, \\ 2\sqrt{-w} \arctan \frac{\sqrt{-w}}{z} & \Leftarrow w < 0. \end{cases} \quad (35)$$

Note that the function G crucially depends on the mass splitting $m_{H^\pm} - m_{H/A}$ and goes to zero in the limit $m_{H^\pm} \approx m_{H/A}$. Hence, within the linear seesaw model, the U parameter is highly suppressed for small v_χ . When U is fixed at zero, the current global fit of electroweak precision data gives [58]:

$$S = 0.00 \pm 0.07, \quad T = 0.05 \pm 0.06. \quad (36)$$

Combining Eq. 32 with Eq. 36, we obtain the following constraint on the mass-splitting:

$$|m_{H^\pm} - m_{H/A}| \leq 80 \text{ GeV at } 90\% \text{ C.L.} \quad (37)$$

On the other hand, a very recent measurement of W boson mass at CDF shows about 7σ deviations from the SM predictions [61]. If one takes this measurement seriously, the global electroweak fit will lead to [62]:

$$S = 0.15 \pm 0.08, \quad T = 0.27 \pm 0.06, \quad (38)$$

with the correlation $\rho_{ST} = 0.93$. Hence, in order to accommodate this new W mass measurement, one needs a sizable central value of the T parameter. The latter is very sensitive to the mass-splitting $m_{H^\pm} - m_{H/A}$ and vanishes for $m_{H^\pm} = m_{H/A}$. As a result, in order to explain the CDF-II measurements the H/A should not be exactly degenerate in mass with H^\pm . We have shown in our previous paper [60] that the W boson mass will be compatible with the CDF-II measurements (at $3\text{-}\sigma$) only when this mass difference lies in the following region:

$$50 \text{ GeV} \leq |m_{H^\pm} - m_{H/A}| \leq 120 \text{ GeV at } 95\% \text{ C.L.} \quad (39)$$

Note that although the absolute scale of the charged Higgs boson mass is not fixed, the CDF-II result suggests that it must lie below a few TeV.

4. CHARGED LEPTON FLAVOUR VIOLATION

The Yukawa interactions are not only responsible for neutrino mass generation, but they also give rise to charged lepton flavour violation (cLFV). In this section we provide the theoretical formulas for the two-body decay amplitudes $\ell_i \rightarrow \ell_j \gamma$. In Fig. 3 we show relevant Feynman diagrams for $\ell_i \rightarrow \ell_j \gamma$ in the mass basis.

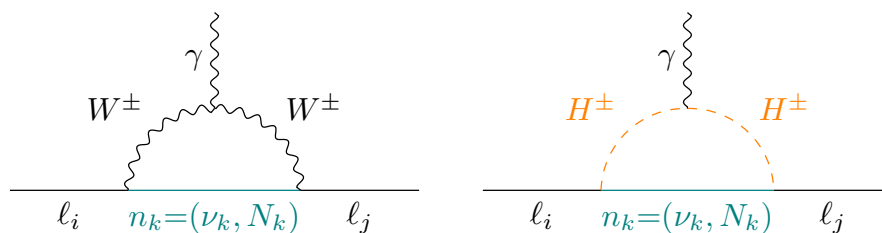


FIG. 3: Feynman diagrams for charged LFV processes e.g. $\ell_i \rightarrow \ell_j \gamma$ present in the model.

The first diagram is the conventional one involving light-heavy neutrino mixing in the effective charged current interactions. Ref. [6] provides a thorough description of the effective lepton mixing matrix K that characterizes the charged current weak interaction of mass-eigenstate neutrinos in any kind of seesaw model. It can be expressed in rectangular form

$$-\mathcal{L}_{\text{CC}} = \frac{g}{2\sqrt{2}} \sum_{\alpha=1}^3 \sum_{\beta=1}^9 K_{\alpha\beta} \bar{\ell}_\alpha \gamma_\mu (1 - \gamma_5) n_\beta W^\mu + \text{H.c.}, \quad (40)$$

where $n_\beta = (\nu, N)$. In the diagonal basis for the charged lepton mass matrix, we can write the K matrix as follows,

$$K = \begin{pmatrix} K_L & K_H \end{pmatrix}, \quad (41)$$

where K_L is a 3 by 3 matrix and K_H is a 3 by 6 matrix. The submatrices K_L and K_H are not unitary. From Eq. 8, we can express K_L and K_H as

$$K_L = \left(1 - \frac{1}{2}m_D M_R^{-1T} M_R^{-1} m_D^\dagger\right) U_{\text{lep}} = \left(1 - \frac{1}{2}V V^\dagger\right) U_{\text{lep}}, \quad (42)$$

$$K_H = \left(-\frac{i}{\sqrt{2}}V \quad \frac{1}{\sqrt{2}}V\right). \quad (43)$$

We parametrize the deviations from unitarity as follows:

$$K_L = (1 - \eta)U_{\text{lep}} \text{ with } \eta = \frac{1}{2}V V^\dagger. \quad (44)$$

For the template scheme with massless neutrinos, these blocks can be parametrized in a very simple manner, see e.g. eqs.(11,12) in [13], because of the high degree of symmetry. It follows that the matrix η characterizes unitarity deviation in the light-active 3×3 sub-block of the lepton mixing matrix³. As this non-unitarity parameter can be relatively large for low-scale seesaw schemes, such as the linear seesaw, it will break the Glashow-Illiopoulos-Maiani (GIM) cancellation mechanism for the light-neutrino contribution [63], see the left panel of Fig. 3. As far as the charged-current interaction is concerned, besides the enhanced light-neutrino contribution, the $\ell_i \rightarrow \ell_j \gamma$ decay also proceeds through the exchange of the six sub-dominantly coupled heavy states [64].

The radiative decay rate is given by [27, 65–68],

$$\text{BR}(\ell_i \rightarrow \ell_j \gamma)_n^{\text{CC}} = \frac{\alpha_w^3 s_w^2}{256\pi^2} \left(\frac{m_{\ell_i}}{M_W}\right)^4 \left(\frac{m_{\ell_i}}{\Gamma_{\ell_i}}\right) \left| \sum_{k=1}^9 K_{ik}^* K_{jk} G_\gamma^W \left(\frac{m_{n_k}^2}{M_W^2}\right) \right|^2, \quad (45)$$

where $\alpha_w = g_w^2/4\pi$, $s_w^2 = \sin^2 \theta_w$. The loop function $G_\gamma^W(x)$ is given as:

$$G_\gamma^W(x) = \frac{1}{12(1-x)^4} (10 - 43x + 78x^2 - 49x^3 + 18x^3 \ln x + 4x^4). \quad (46)$$

In order to examine the variation of the cLFV rates in parameter space we perform a scan procedure using the approximate Casas-Ibarra-like expression [69] of the Dirac Yukawa couplings in terms of oscillation parameters given as [64, 70, 71],

$$Y_\nu = \frac{\sqrt{2}}{v_\Phi} U_{\text{lep}} \text{diag}\{\sqrt{m_i}\} \mathcal{A}^T \text{diag}\{\sqrt{m_i}\} U_{\text{lep}}^T (M_L^T)^{-1} M_R^T, \quad (47)$$

³ For high scale type-I seesaw, the deviations from unitarity are negligible, $V \sim 10^{-10}$, however they can lead to a rich phenomenology in low-scale seesaw.

where U_{lep} is approximately the mixing matrix determined in oscillation experiments [72], m_i are the three light neutrino masses and \mathcal{A} has the following general form:

$$\mathcal{A} = \begin{pmatrix} \frac{1}{2} & a & b \\ -a & \frac{1}{2} & c \\ -b & -c & \frac{1}{2} \end{pmatrix}, \quad (48)$$

with a, b, c are real numbers. Using this analytical parametrization optimizes the scan, ensuring that only viable solutions consistent with oscillation data are included. Having said that, we stress that in the numerical code, the exact expressions are used in order to “extract” the Yukawas from the measured neutrino observables.

Parameter	Range
m_{H^\pm}	[100, 2000] GeV
M_{N_i}	[1, 100] TeV
a, b, c	[0, 10^{-2}]
α	$[-\frac{\pi}{2}, \frac{\pi}{2}]$
v_χ	[10^{-9} , 1] GeV
Y_S^{ii}	[10^{-4} , $\sqrt{4\pi}$]

TABLE II: Parameter range used for the numerical scan of cLFV processes.

In Fig. 4, we show the charged current contribution to the $\mu \rightarrow e\gamma$ rate involving light neutrinos (blue) and heavy neutrinos (orange) as a function of the relevant unitarity violation parameter η varying the parameter space according to Table. II. As η is a 3×3 matrix, we choose to show the results in terms of the parameter $\text{Tr}(\eta)$. From Fig. 4, one sees that the light neutrino contribution (blue points) can exceed that coming from the heavy neutrinos (orange points). It is clear from this figure that the charged current contribution need not be suppressed by the small neutrino masses, and can lead to observable rates even in the limit of vanishing v_χ as neutrinos become massless [26, 28–32]. The GIM cancelation is broken in the light neutrino sector due to the non-unitarity of the leptonic mixing matrix. In particular, the contribution involving light neutrino exchange can be as large as that coming from heavy neutrinos.

Notice that cLFV processes also receive contributions coming from the Yukawa interac-

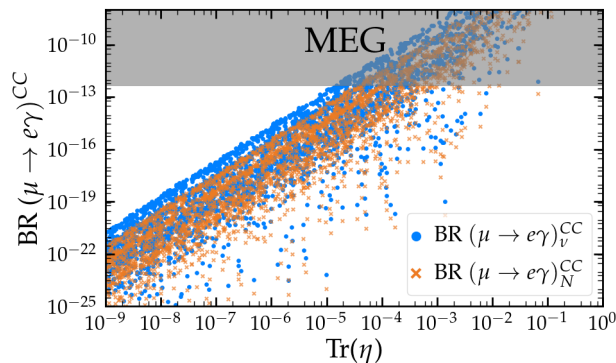


FIG. 4: Charged current contribution to $\mu \rightarrow e\gamma$ as a function of the unitarity violation parameter η . A full calculation is performed varying the parameters described in Table II as explained in the text. The horizontal band is excluded by the MEG experiment [43].

tions. The relevant Yukawa interactions are given as

$$- \mathcal{L}_N^{\text{Yuk}} \approx \frac{\sin \beta}{2\sqrt{2}} \sum_{\alpha,\beta=1}^3 Y_S^{\alpha\beta} \bar{\ell}_\alpha (1 + \gamma_5) (iN_{2\beta+2} + N_{2\beta+3}) H^- + \text{H.c.}, \quad (49)$$

$$- \mathcal{L}_\nu^{\text{Yuk}} \approx \frac{v \sin^2 \beta}{2\sqrt{2}} \sum_{\alpha,\beta=1}^3 (Y_S M_R^{-1} Y_\nu^\dagger)_{\alpha\beta} \bar{\ell}_\alpha (1 + \gamma_5) \nu_\beta H^- + \text{H.c.} \quad (50)$$

The individual contributions to the rate for the radiative $\ell_i \rightarrow \ell_j \gamma$ decay coming from these Yukawa terms is given by [73],

$$\text{BR}(\ell_i \rightarrow \ell_j \gamma)_N^{\text{Yuk}} = \frac{\alpha_{\text{em}}}{4} \left(\frac{m_{\ell_i}^5}{\Gamma_{\ell_i}} \right) \left| (Y_p Y_p^\dagger)_{ji} I_p \left(M_{H^\pm}, \frac{M_N^2}{M_{H^\pm}^2} \right) \right|^2, \quad (51)$$

$$\text{BR}(\ell_i \rightarrow \ell_j \gamma)_\nu^{\text{Yuk}} = \frac{1}{(192\pi^2 M_{H^\pm}^2)^2} \frac{\alpha_{\text{em}}}{4} \left(\frac{m_{\ell_i}^5}{\Gamma_{\ell_i}} \right) \left| \frac{v^2 \sin^4 \beta}{2M_N^2} (Y_S Y_\nu^\dagger Y_\nu Y_S^\dagger)_{ji} \right|^2, \quad (52)$$

where $\alpha_{\text{em}} = e^2/4\pi$ and $Y_P = Y_S \sin \beta$. The loop function $I_p(m_B, x)$ has the following form:

$$I_p(m_B, x) = -\frac{1}{16\pi^2 m_B^2} \left(\frac{(3x-1)}{4(x-1)^2} - x^2 \frac{\log x}{2(x-1)^3} \right) + \frac{3}{32\pi^2 m_B^2} \left(\frac{11x^2 - 7x + 2}{18(x-1)^3} - x^3 \frac{\log x}{3(x-1)^4} \right). \quad (53)$$

In Fig. 5 and 6, we show the resulting cLFV decay rates as a function of the relevant parameters, varied according to Table. II. We impose the additional constraint of perturbativity of the Yukawa couplings Y_ν and Y_S . Notice that in the limit $v_\chi \rightarrow 0$, $M_L \rightarrow 0$, neutrinos are massless and the Yukawa coupling Y_ν becomes unrestricted by neutrino mass limits. The latter affects the magnitude of M_L , which can be dynamically suppressed by

v_χ even if the Yukawa couplings Y_ν and Y_S are sizeable. As a result one can have large contributions to cLFV from charged current interaction. This is indeed confirmed in Fig. 5, that shows the total $\mu \rightarrow e\gamma$ rate as a function of v_χ .

As noted long ago [26, 28–32], the fact that the charged-current contributions to cLFV can

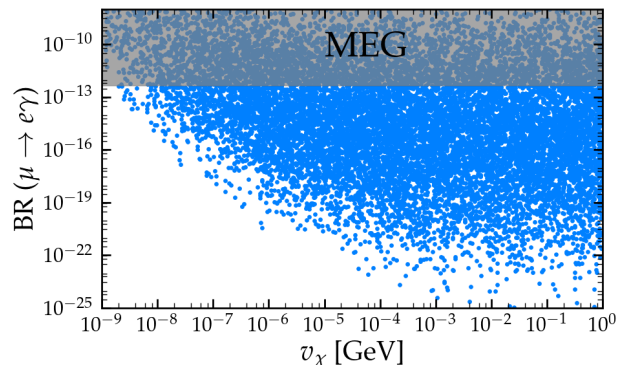


FIG. 5: Total $\text{BR}(\mu \rightarrow e\gamma)$ as a function of v_χ . We have varied the parameters according to Table II as explained in the text. The upper band indicates the limit from the MEG experiment [43].

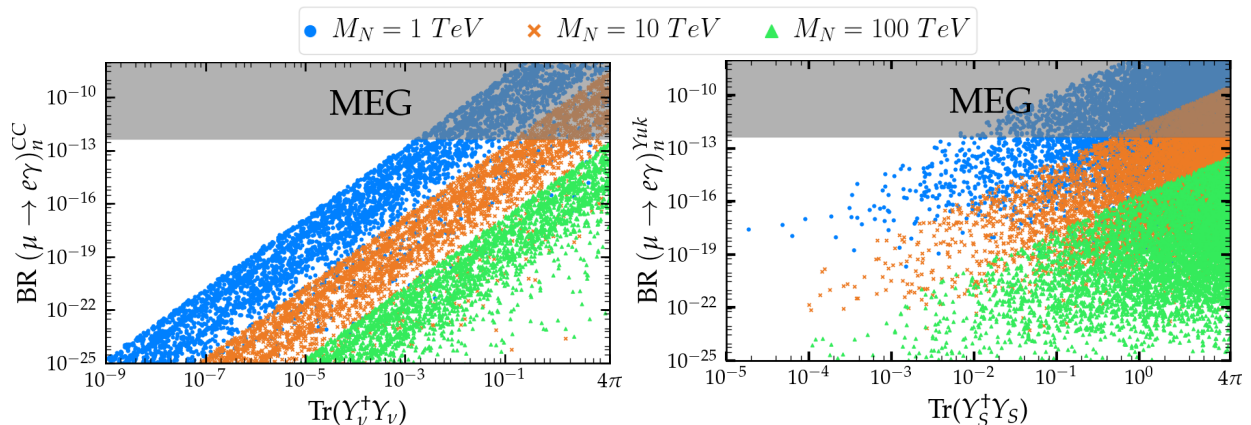


FIG. 6: $\text{BR}(\mu \rightarrow e\gamma)$ for various mediator mass values M_N . Left panel: Charged current contribution versus $\text{Tr}(Y_\nu^\dagger Y_\nu)$. Right panel: Yukawa contribution versus $\text{Tr}(Y_S^\dagger Y_S)$. The horizontal band indicates the limit from the MEG experiment [43]. The charged Higgs boson mass is taken as $m_{H^\pm} = 100$ GeV, 1 TeV and 2 TeV (blue, orange and green points, respectively). Other parameters are varied as in Table II.

be sizeable is a generic feature of low-scale seesaw mechanisms, including also the inverse seesaw mechanism [7, 8]. A novel feature of the linear seesaw is the presence of a second Yukawa interaction characterized by the coupling matrix Y_S and involving a second doublet Higgs scalar. Indeed, this Yukawa coupling Y_S can be sizeable for small v_χ , as it is not directly restricted by the neutrino mass constraint. In the left and right panels of Fig. 6, we show the total $\text{BR}(\mu \rightarrow e\gamma)$ as a function of $\text{Tr}(Y_\nu^\dagger Y_\nu)$ and $\text{Tr}(Y_S^\dagger Y_S)$, respectively. One sees

that the Yukawa contributions to the $\mu \rightarrow e\gamma$ decay rate can exceed those of the charged current and also exceed the present experimental bound from the MEG experiment [43] for reasonable choices for the Yukawa couplings Y_ν and Y_S .

In summary, as the main message, we stress that the rates for cLFV processes need not be “neutrino-mass-suppressed” so that cLFV processes can be non-zero even in the massless neutrino limit. Moreover, the linear seesaw framework brings in novel and potentially dominant cLFV contributions associated with the Yukawa sector and the charged scalar boson.

Before closing, we comment on another class of relevant processes, involving (total) lepton number violation, such as neutrinoless double beta decay ($0\nu\beta\beta$). In addition to light and heavy neutrino contributions, within the linear seesaw model there will be a contribution to $0\nu\beta\beta$ from the charged Higgs boson exchange. However, very much like the charged-Higgs-boson contribution [74] present in the triplet seesaw mechanism [6], the charged-Higgs-boson of the linear seesaw is also strongly “leptophilic” in the small v_χ limit, leading to a negligible contribution to $0\nu\beta\beta$. See Ref. [75] for further discussion on lepton number violating processes.

5. COLLIDER CONSTRAINTS

At the LHC, the additional neutral Higgs scalars H and A are produced dominantly through gluon-gluon fusion, generated by top (t) and bottom (b) quark exchange in the loops [76, 77]. The CMS and ATLAS collaborations have searched for such new scalars decaying to various SM channels. The official CMS and ATLAS searches [78–80] employ $gg \rightarrow tbH^\pm$ and $gb \rightarrow tH^\pm$ as the production channels for the singly charged Higgs. However, within our linear seesaw model, the relevant couplings involved in these processes are suppressed as $\mathcal{O}(v_\chi/v)$, hence these constraints are not directly applicable.

The LEP experiments have looked for pair production of charged Higgs bosons through the process $e^+e^- \rightarrow \gamma/Z \rightarrow H^\pm H^\mp$. Although the couplings that appear in the production process are gauge couplings, the H^\pm decay to hadronic states are again suppressed as $\mathcal{O}(v_\chi/v)$ [81]. In conclusion, due to the suppressed H, A and H^\pm couplings to SM particles, all the constraints coming from searches for additional scalars at LHC and LEP can be easily satisfied. Thus H, A and H^\pm are allowed to have broad mass ranges.

Moreover, the precise measurements of the W and Z widths at LEP require [82, 83]:

$$m_H + m_A, 2m_{H^\pm} > m_Z, \text{ and } m_{H/A} + m_{H^\pm} > m_W. \quad (54)$$

In the limit $v_\chi \rightarrow 0$, α and β can be approximated as $\alpha \approx 0$ and $\beta \approx \pi/2$. Therefore, Φ behaves almost identically to the SM Higgs doublet, so we do not anticipate any observable

deviation from the Higgs couplings to the SM particles. A possible exception are loop-induced couplings, such as $h\gamma\gamma$, to which we turn next.

Constraints from Higgs Physics

The $h \rightarrow \gamma\gamma$ decay width is modified in the linear seesaw model due to the existence of a new physical charged scalar H^+ running in the loop as shown in Fig. 7.

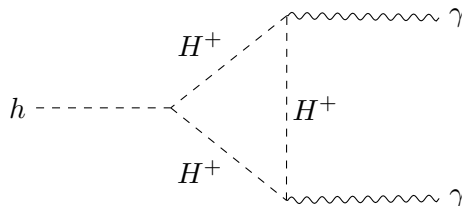


FIG. 7: $h \rightarrow \gamma\gamma$ process mediated by the new charged scalar H^+ running in the loop.

The $h \rightarrow \gamma\gamma$ decay width including this new contribution can be written as [84, 85]

$$\Gamma(h \rightarrow \gamma\gamma) = \frac{G_\mu \alpha^2 m_h^3}{128 \sqrt{2} \pi^3} \left| \sum_f g_f N_c Q_f^2 A_{1/2}^h(\tau_f) + g_W A_1^h(\tau_W) + g_h A_0^h(\tau_{H^\pm}) \right|^2, \quad (55)$$

where

$$g_W = \sin(\beta - \alpha), \quad g_f = \frac{\cos \alpha}{\sin \beta}, \quad g_h = -\frac{m_W}{g m_{H^\pm}^2} \lambda_{hH^+H^+}. \quad (56)$$

Q_f and N_c are the electric charge and colour of the fermion f , while g is the weak coupling constant and $\lambda_{hH^+H^+}$ is the trilinear hH^+H^+ coupling,

$$\lambda_{hH^+H^+} = -\frac{1}{2v \sin(2\beta)} [(m_h^2 - 2m_{H^\pm}^2) \cos(\alpha - 3\beta) + (3m_h^2 + 2m_{H^\pm}^2 - 4m_A^2) \cos(\alpha + \beta)]. \quad (57)$$

Notice that, among all SM fermions f , the dominant contribution comes from the top quark, followed by a small bottom-quark contribution. The form factors $A_{1/2}^h$, A_1^h and A_0^h are given as

$$\begin{aligned} A_{1/2}^h(\tau) &= 2[\tau + (\tau - 1)f(\tau)] \tau^{-2}, \\ A_1^h(\tau) &= -[2\tau^2 + 3\tau + 3(2\tau - 1)f(\tau)] \tau^{-2}, \\ A_0^h(\tau) &= -[\tau - f(\tau)] \tau^{-2}, \end{aligned} \quad (58)$$

where $\tau_i = M_h^2/4M_i^2$; $i = f, W, H^\pm$ with M_i denoting the mass of the particle running in the

$h \rightarrow \gamma\gamma$ loop, and the function $f(\tau)$ is defined as:

$$f(\tau) = \begin{cases} \arcsin^2 \sqrt{\tau} & \tau \leq 1 \\ -\frac{1}{4} \left[\log \frac{1 + \sqrt{1 - \tau^{-1}}}{1 - \sqrt{1 - \tau^{-1}}} - i\pi \right]^2 & \tau > 1 \end{cases} \quad (59)$$

To quantify the deviation from the Standard Model prediction, we define the following parameter

$$R_{\gamma\gamma} = \frac{\text{BR}(h \rightarrow \gamma\gamma)}{\text{BR}(h \rightarrow \gamma\gamma)_{\text{SM}}}. \quad (60)$$

The value we use for the Standard Model is $\text{BR}(h \rightarrow \gamma\gamma)_{\text{SM}} \approx 2.27 \times 10^{-3}$. This decay mode has been explored by the ATLAS and CMS collaborations, and their combined study of the 8 TeV data yields $R_{\gamma\gamma}^{\text{exp}} = 1.16_{-0.18}^{+0.20}$ [86]. There is currently no combined final data for the 13 TeV Run-2, and the available data is separated by the production process [87]. In our analysis we use the 13 TeV ATLAS result which gives the global signal strength measurement of $R_{\gamma\gamma}^{\text{exp}} = 1.04_{-0.09}^{+0.10}$ [88].

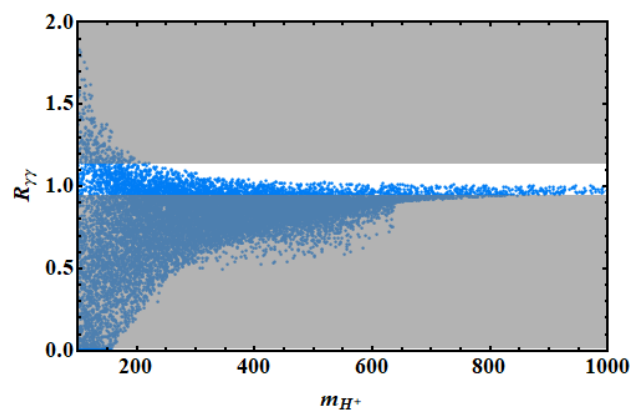


FIG. 8: Dependence of the diphoton signal strength $R_{\gamma\gamma}$ on the charged scalar mass. For $v_\chi \in [10^{-9}, 10]$ GeV we varied the other relevant parameters as $m_{H^\pm}, m_{H/A} \in [100, 2000]$ and $\alpha \in [-\frac{\pi}{2}, \frac{\pi}{2}]$. The shaded regions are excluded from the experimental limits on $R_{\gamma\gamma}$ [88].

Fig. 8 shows a scatter plot of $R_{\gamma\gamma}$ as a function of m_{H^\pm} . One sees that no charged-Higgs mass values can be ruled out from the experimental limits on $R_{\gamma\gamma}$ from ATLAS [88].

6. PRODUCTION OF HEAVY NEUTRINOS AND NEW SCALARS

Within our linear seesaw scheme, the heavy neutrino mediators N_i as well as the new scalars H, A, H^\pm can all naturally lie below the TeV scale, hence accessible to direct experimental discovery at future particle colliders. The possibility of producing the heavy neutrinos that mediate neutrino mass generation at high energy colliders [20–22] has a long history [13–19, 89–96].

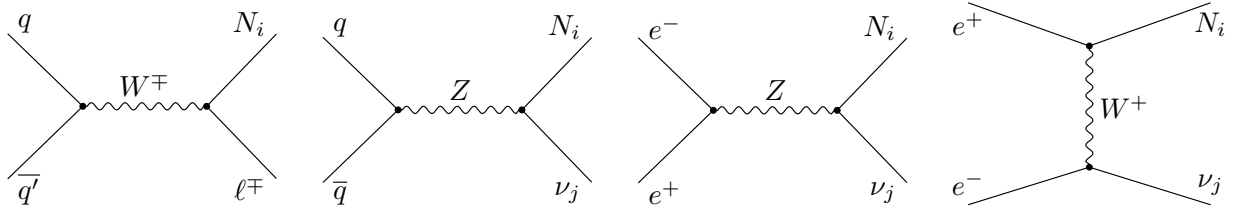


FIG. 9: Feynman diagrams for single heavy neutrino production through the SM gauge portal at pp and e^+e^- colliders. However, these channels are suppressed by light-heavy neutrino mixing.

Indeed, heavy neutrino mediators can be produced at proton-proton or e^+e^- colliders in a variety of ways. At pp colliders, the most studied production mechanism is the charged- and neutral-current-induced Drell-Yan process, $pp \rightarrow W^{\pm*} \rightarrow \ell^{\pm}N$ and $pp \rightarrow Z^* \rightarrow \nu N$, see Fig. 9. At e^+e^- colliders, the heavy neutrinos can be singly-produced as $e^+e^- \rightarrow \nu N$ through gauge-mediated t and s-channel processes, see Fig. 9. However, barring resonant production [13], the heavy neutrino's production cross-section is very small due to light-heavy neutrino mixing suppression ($\mathcal{O}(m_D M_R^{-1})$ in the amplitude).

In what follows we discuss the new unsuppressed production mechanisms for neutrino mass mediators within our linear seesaw scheme. We show how they could produce interesting distinctive signatures at various collider setups.

6.1. Direct heavy-neutrino pair production at e^+e^- collider

Our linear seesaw scheme offers new unsuppressed heavy-neutrino production mechanisms. For example, as illustrated in the right panel of Fig. 10, heavy neutrinos can be produced as $e^+e^- \rightarrow NN$ through t-channel exchange of the charged Higgs boson. In contrast to the first two diagrams in Fig. 10 which are light-heavy neutrino mixing suppressed, the contribution to the production cross section arising from the Higgs exchange diagram in Fig. 10 is proportional to Y_S^4 . As we already discussed, for small v_χ , sizeable Y_S values

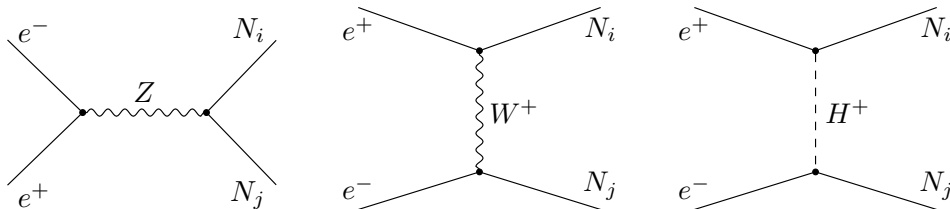


FIG. 10: Feynman diagrams for heavy-neutrino pair production at an e^+e^- collider. The gauge diagrams are suppressed by light-heavy neutrino mixing (first two panels) while the t-channel scalar exchange diagram is unsuppressed (last panel).

are consistent with small neutrino masses. The analytical expression for this production

cross-section is given explicitly as

$$\frac{d\sigma}{d\cos\theta} = \frac{|Y_S^{1i}|^4}{256\pi\sqrt{s}} \frac{(s - 4M_{N_i}^2)^{\frac{3}{2}}}{\left((2m_{H^\pm}^2 - 2M_{N_i}^2 + s)^2 - s\cos^2\theta(s - 4M_{N_i}^2)^2 \right)^2} \left[2\cos^2\theta \left(2(m_{H^\pm}^2 - M_{N_i}^2) - s^2 - 2s(m_{H^\pm}^2 - 2M_{N_i}^2) \right) + (s + 2m_{H^\pm}^2 - 2M_{N_i}^2)^2 + s\cos^4\theta(s - 4M_{N_i}^2) \right], \quad (61)$$

where \sqrt{s} and θ are the CM energy and scattering angle. One sees from Eq. 61 that, for

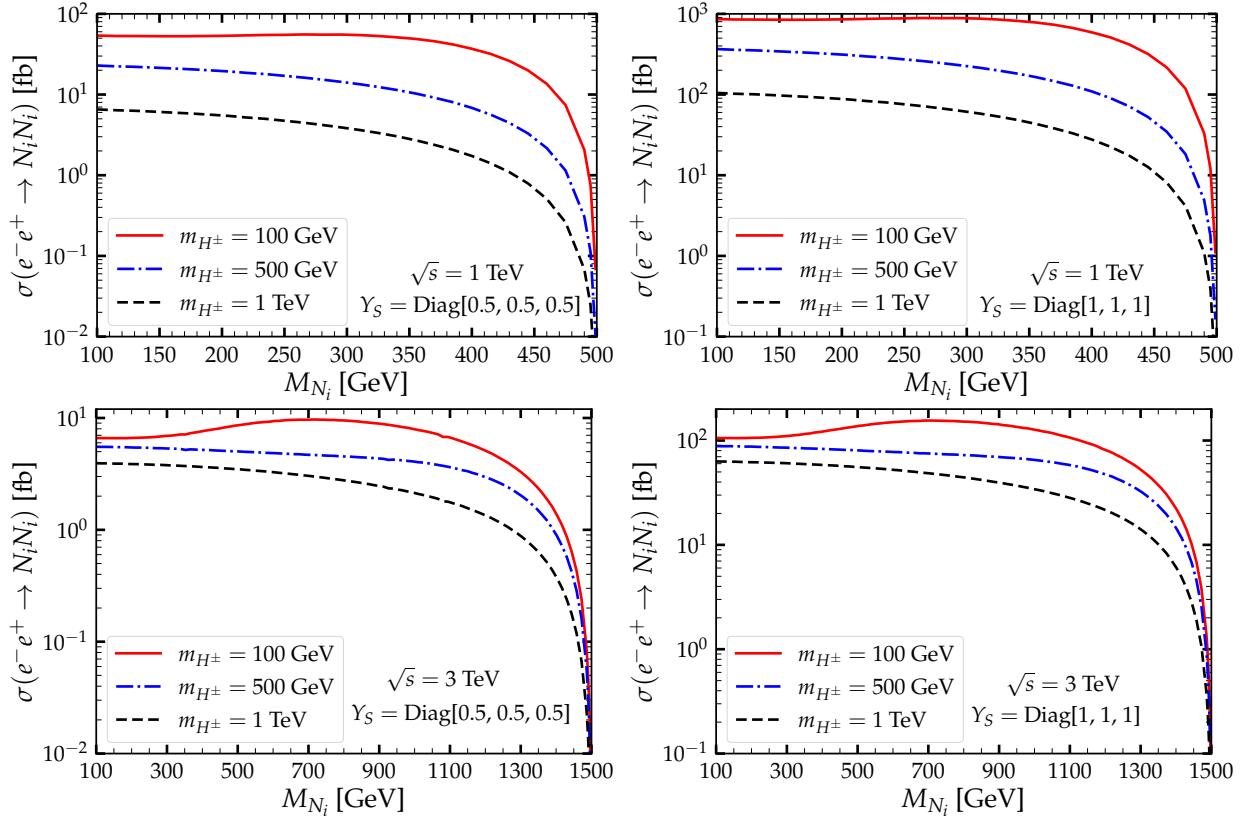


FIG. 11: Cross-section for heavy-neutrino pair production versus its mass M_{N_i} at an e^+e^- collider with center of mass energy $\sqrt{s} = 1$ TeV (top) and $\sqrt{s} = 3$ TeV (bottom). Results are shown for different Y_S and charged-Higgs boson mass values, as indicated.

adequately large but experimentally allowed values of the Yukawa coupling Y_S , the process $e^+e^- \rightarrow NN$ provides a promising way to produce heavy neutrinos. In Fig. 11 we display the heavy-neutrino pair-production cross-section $\sigma(e^+e^- \rightarrow N_i N_i)$ for two benchmark Yukawa couplings $Y_S = \text{Diag}(0.5, 0.5, 0.5)$ (left panels) and $Y_S = \text{Diag}(1, 1, 1)$ (right panels) for center of mass energy $\sqrt{s} = 1$ TeV (top panels) and $\sqrt{s} = 3$ TeV (bottom panels). The three lines in each panel correspond to three charged-Higgs masses $m_{H^\pm} = 100$ GeV, 500 GeV and 1000 GeV. One can clearly see that a relatively large Yukawa coupling Y_S leads to a sizeable t-channel cross section. Therefore, from this discussion it follows that heavy-

neutrino pair-production at e^+e^- colliders deserves further study to ascertain the potential detectability of the associated signatures.

6.2. Heavy neutrino production associated with charged Higgs at $e^- \gamma$ collider

In the context of e^+e^- colliders, the e^+ beam can be replaced by a back-scattered photon, leading to an $e^- \gamma$ collider which can have extremely rich physics potential [47–52]. Within our linear seesaw setup an $e^- \gamma$ collider can also produce the heavy neutrino mediator in association with the charged Higgs boson. The relevant Feynman diagrams for this process are shown in Fig. 12. Notice that the first diagram is suppressed by light-heavy neutrino mixing, whereas the last two diagrams are proportional to Y_S^2 . Hence, for relatively large Y_S , we also expect to have large cross section for this process.

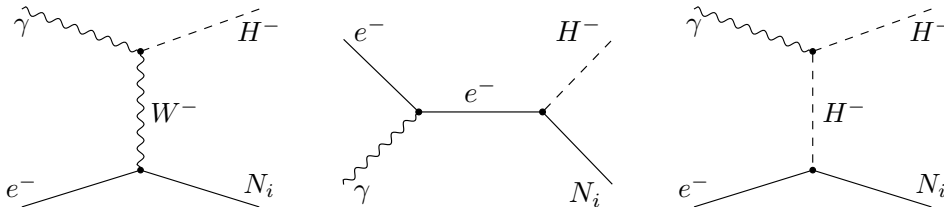


FIG. 12: Feynman diagrams for NH^- production at an $e^- \gamma$ collider. The first diagram is light-heavy neutrino mixing suppressed.

The analytical expression for this production cross-section is given as

$$\frac{d\sigma}{d\cos\theta} = \frac{\alpha_{\text{em}} |Y_S^{1i}|^2}{16s^2 (m_{H^\pm}^2 - t)^2} \lambda^{\frac{1}{2}} \left(1, \frac{M_{N_i}^2}{s}, \frac{m_{H^\pm}^2}{s} \right) \left[t(2M_{N_i}^4 - 2M_{N_i}^2(s+t) + t(s+t)) - m_{H^\pm}^2(2M_{N_i}^4 + t^2) + m_{H^\pm}^4(2M_{N_i}^2 + s+t) - m_{H^\pm}^6 \right], \quad (62)$$

with $t = -\frac{1}{2}(s - M_{N_i}^2 - m_{H^\pm}^2) + \frac{\cos\theta}{2} \lambda^{\frac{1}{2}}(s, M_{N_i}^2, m_{H^\pm}^2)$. Using Eq. 62 we obtain Fig. 13, which shows the $N_i H^-$ production cross section versus M_{N_i} (left panels) and m_{H^\pm} (right panels) for center of mass energy $\sqrt{s} = 1$ TeV (top panels) and $\sqrt{s} = 3$ TeV (bottom panels). For all panels we fix the Yukawa coupling to be $Y_S = \text{Diag}(1, 1, 1)$. The three lines in the left panels (right panels) correspond to three values of charged Higgs (heavy neutrino) mass $m_{H^\pm}(M_{N_i}) = 100$ GeV, 200 GeV and 500 GeV for the top panels and $m_{H^\pm}(M_{N_i}) = 100$ GeV, 500 GeV and 1000 GeV for the bottom panels. Comparing different lines in Fig. 13, we see that the cross-section tends to increase with the heavy neutrino mass M_{N_i} , provided the phase-space is sufficiently open (left panels). This behavior can also be seen in Fig. 14, where we compare the leading contributions coming from s- and t-channels in Fig. 12, as well as the interference between them.

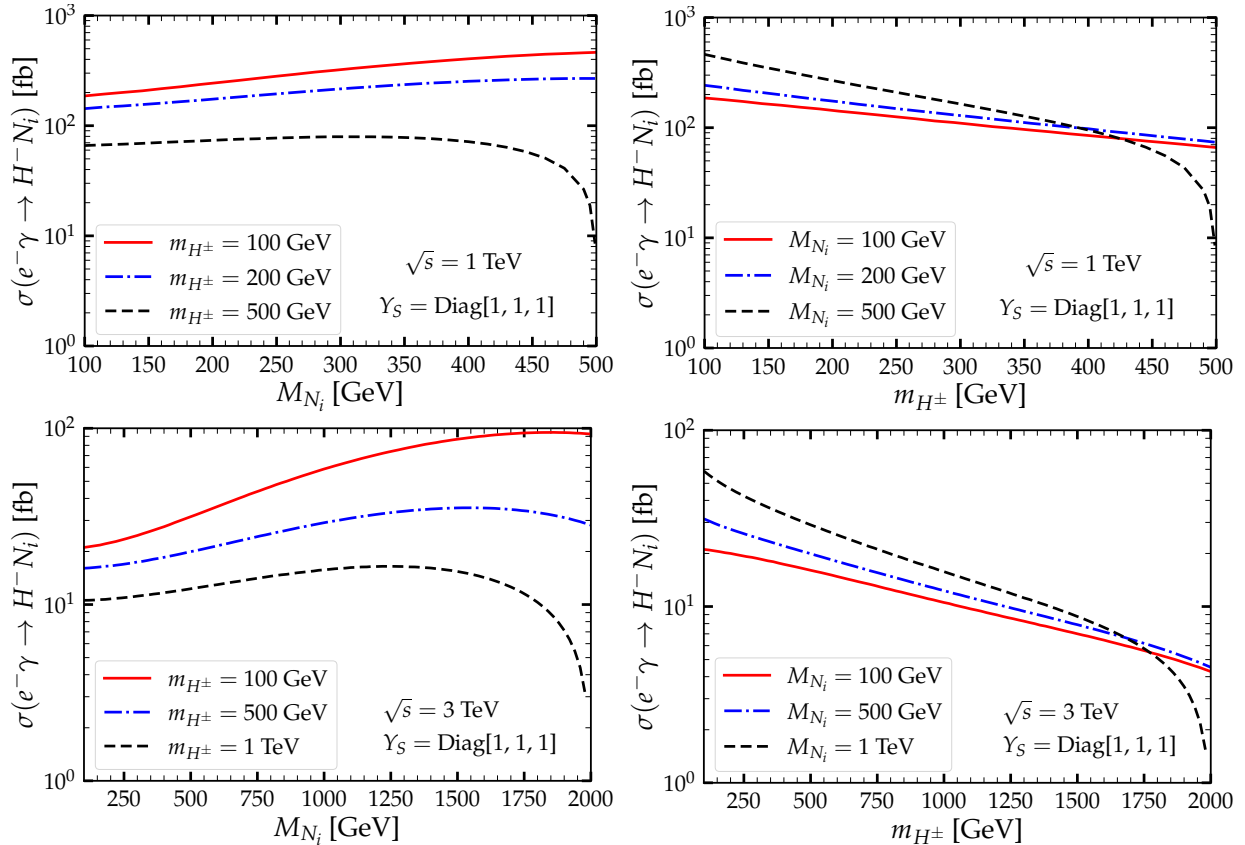


FIG. 13: NH^- production cross-section versus the heavy neutrino mass M_{N_i} (left panel) and versus the charged scalar mass m_{H^\pm} (right panel) at an $e^- \gamma$ collider at center of mass energy $\sqrt{s} = 1$ TeV (top) and $\sqrt{s} = 3$ TeV (bottom). Left panels (right panels) correspond to three values of the charged Higgs (heavy neutrino) mass $m_{H^\pm}(M_{N_i}) = 100$ GeV, 200 GeV and 500 GeV for the top panels, and $m_{H^\pm}(M_{N_i}) = 100$ GeV, 500 GeV and 1000 GeV for the bottom panels.

The left and right panels in Fig. 14 correspond to two different charged Higgs masses, $m_{H^\pm} = 100$ GeV and $m_{H^\pm} = 1$ TeV, respectively. From the left panel, we see that for lighter charged Higgs mass $m_{H^\pm} = 100$ GeV, the t-channel contribution dominates over s-channel and grows with heavy neutrino mass M_{N_i} , leading to the rising trend of the total cross-section with M_{N_i} . For larger charged Higgs mass $m_{H^\pm} = 1$ TeV, the t-channel and s-channel contributions are of the same order, and the t-channel contribution does not grow with heavy neutrino mass M_{N_i} due to the phase space suppression. This is why the cross-section in Fig. 13 grows with mass M_{N_i} for light charged Higgs but decreases when the charged Higgs or heavy neutrino become heavy enough to suppress the phase space. Note however that, even in the idealized limit of infinite energy (corresponding to a collider with infinite \sqrt{s} energy) the cross-section will ultimately stop growing owing to the unitarity of the theory.

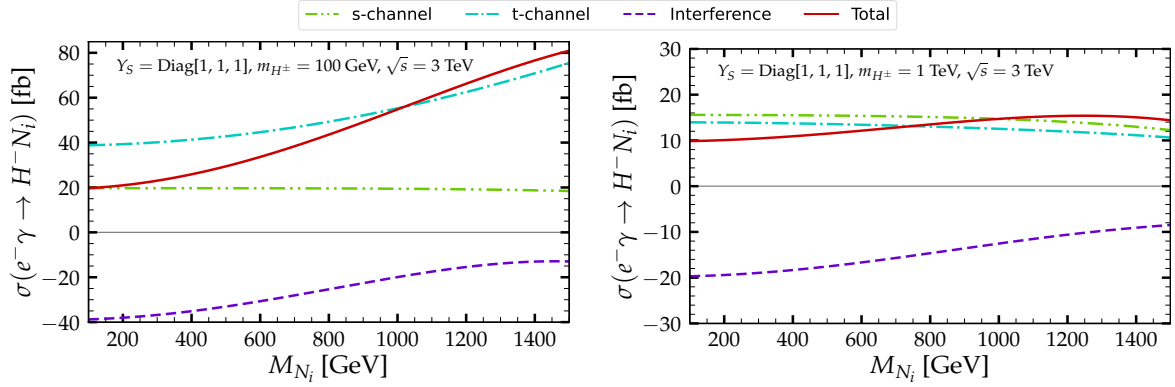


FIG. 14: Comparison of individual contributions to the cross-section for the process $e^- \gamma \rightarrow N_i H^-$ at center of mass energy $\sqrt{s} = 3$ TeV. Left (right) panels correspond to charged Higgs masses $m_{H^\pm} = 100$ GeV (1 TeV). See text for details.

6.3. Heavy neutrinos from charged-scalar pair and associated pair production

In contrast to the inverse seesaw, the presence of a charged Higgs boson in our linear seesaw is a key feature required in order to seed the neutrino mass, see Eqs. 4 and 12. This brings in the possibility of producing the heavy neutrinos via the charged and neutral Higgs boson decays.

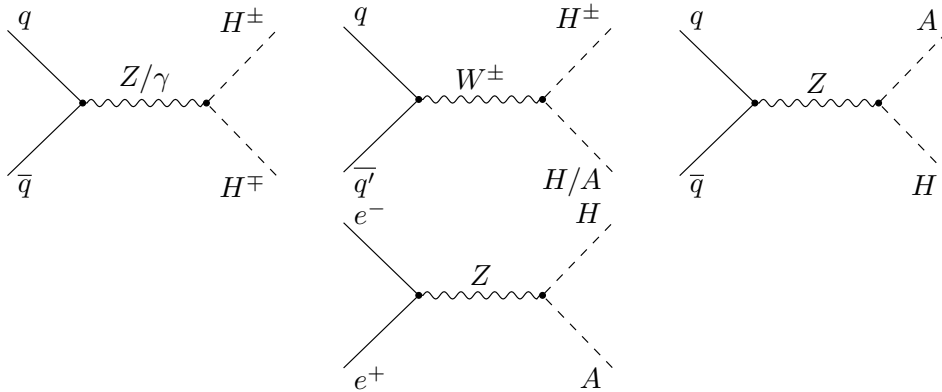


FIG. 15: Feynman diagrams for Drell-Yan Higgs boson production at pp (upper panel) and e^+e^- (bottom panel) colliders. Charged Higgs production at an e^+e^- collider is discussed separately below, see Fig. 17, 18 and the accompanying discussion.

Indeed, the decays of such Higgs bosons to the heavy neutrinos are not suppressed by the light-heavy neutrino mixing. This is because the pair production and associated production of scalars $\Phi\Phi'$ (with $\Phi, \Phi' \in \{H, A, H^\pm\}$) via the neutral or charged current Drell-Yan mechanism involving s-channel $\gamma/Z, W^\pm$ exchange (see Fig. 15) can be large. In Fig. 16 we display these cross-sections both at pp ($\sqrt{s} = 14$ TeV, 100 TeV) as well as e^+e^- colliders ($\sqrt{s} = 1$ TeV, 3 TeV). One sees that at such large center of mass energies the production cross section is large enough that multi-TeV Higgs masses can be explored.

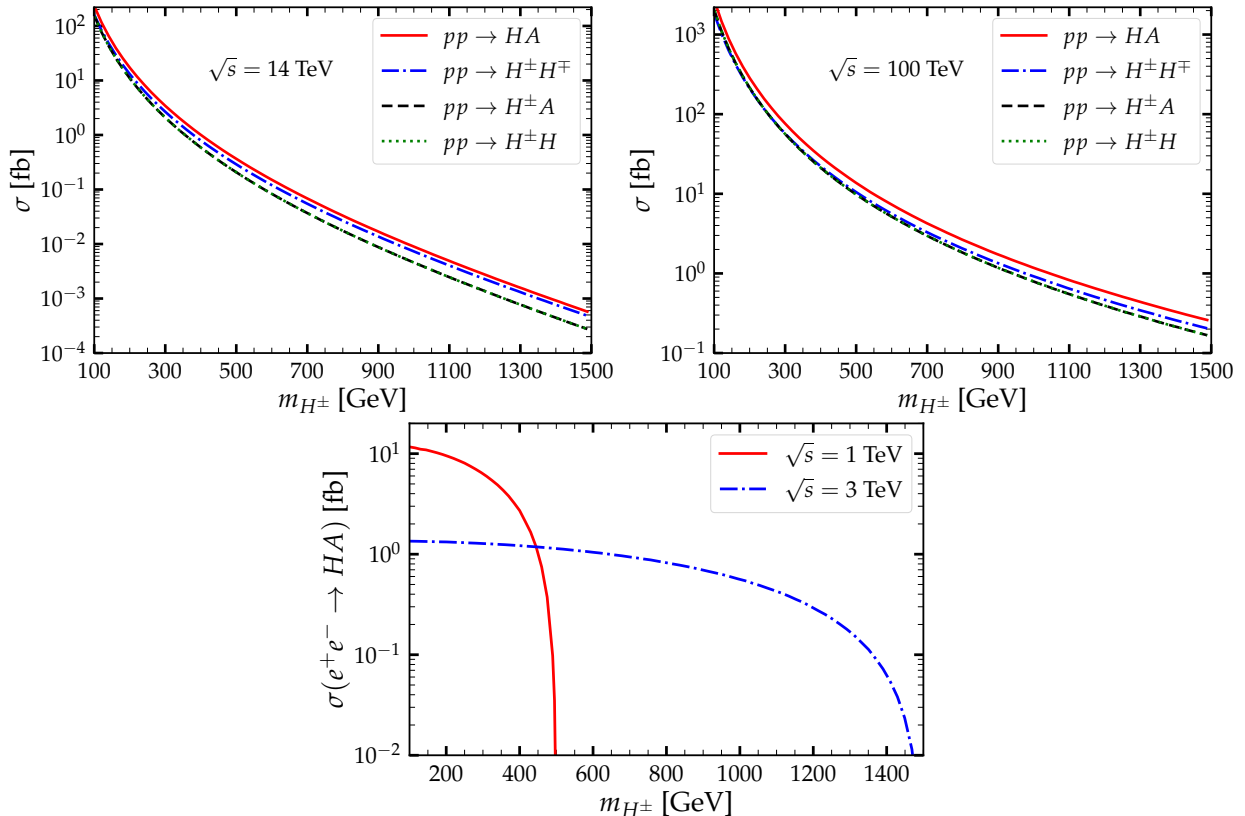


FIG. 16: Cross section for pair and associated production of new scalars vs the charged scalar mass at pp (upper panel) and e^+e^- (bottom panel) colliders. We took center of mass energies $\sqrt{s} = 14$ TeV (left panel) and $\sqrt{s} = 100$ TeV (right panel) for pp colliders and $\sqrt{s} = 1$ TeV (red line) and $\sqrt{s} = 3$ TeV (blue line) for the e^+e^- collider. These results assume $m_{H^\pm} \approx m_H \approx m_A$, in agreement with the constraints discussed in previous sections.

Beyond Drell-Yan production, in the linear seesaw, one can have heavy-neutrino-mediated t-channel charged Higgs boson pair-production, as shown in Fig. 17. This new process is a characteristic feature of e^+e^- colliders, absent at pp colliders. The contribution from the

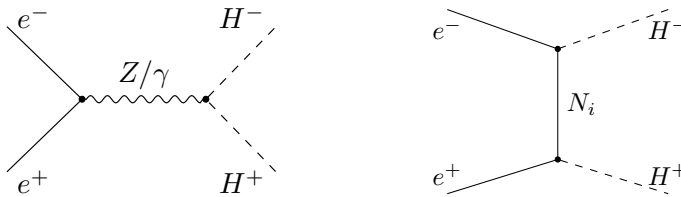


FIG. 17: Feynman diagrams for the charged Higgs production in an e^+e^- collider. Left panel: Drell-Yan production. Right panel: t-channel heavy neutrino mediated production.

t-channel exchange of heavy neutrinos is proportional to Y_S^4 . Hence, for relatively large Y_S , this production cross section can be large and can even surpass the Drell-Yan production.

The analytical expression for this contribution to the production cross-section is given as

$$\frac{d\sigma}{d\cos\theta} = \frac{|Y_S^{1i}|^4 \sin^2\theta (s - 4m_{H^\pm}^2)^{\frac{3}{2}}}{128\pi\sqrt{s} \left(s + 2M_{N_i}^2 - 2m_{H^\pm}^2 + \cos\theta \sqrt{s(s - 4m_{H^\pm}^2)} \right)^2}. \quad (63)$$

In Fig. 18, we compare the Drell-Yan contribution with the t-channel contribution for this production channel. The left and right panels correspond to two different choices of Yukawa

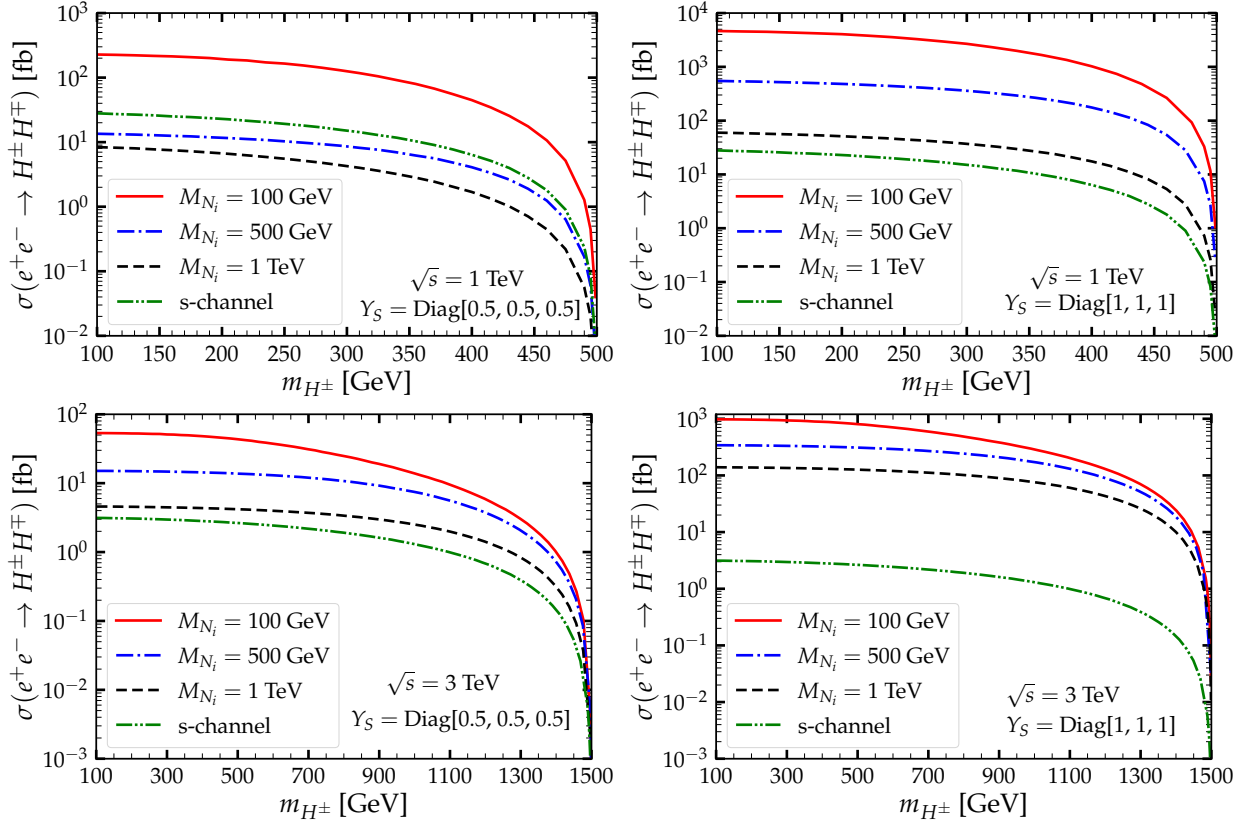


FIG. 18: Cross-section for the charged scalar pair production in an e^+e^- collider at center of mass energy $\sqrt{s} = 1$ TeV (top) and $\sqrt{s} = 3$ TeV (bottom) versus the charged scalar mass. The green line represents the s-channel contribution only, whereas the other three lines include both the s- and the t-channel. They correspond to three mediator masses, $M_{N_i} = 100$ GeV, 500 GeV, and 1 TeV. Left and right panels assume Y_S as $\text{Diag}(0.5, 0.5, 0.5)$ and $\text{Diag}(1, 1, 1)$, respectively.

couplings $Y_S = \text{Diag}(0.5, 0.5, 0.5)$ and $Y_S = \text{Diag}(1, 1, 1)$. The top and bottom panels correspond to two different choices of center of mass energies $\sqrt{s} = 1$ TeV and $\sqrt{s} = 3$ TeV, respectively. In each panel, the double-dotted dashed green line gives the pure Drell-Yan contribution, whereas the other three lines give the combined contribution coming from Drell-Yan and t-channel heavy neutrino mediation for three benchmark values of the heavy neutrino mass $M_{N_i} = 100$ GeV, 500 GeV and 1 TeV. One sees that there is a substantial enhancement in the cross-section once the t-channel contribution is included along with the

Drell-Yan contribution.

Before closing this section, we would like to stress that once the new charged and neutral Higgs bosons are produced at a pp or e^+e^- collider, the heavy seesaw mediator neutrinos can be generated from their decays, such as $H^\pm \rightarrow \ell^\pm N_i$ or $H/A \rightarrow \nu N$. Hence this will effectively enhance the heavy neutrino production. The pair-production cross-section of the charged scalar at a hadron collider becomes smaller for large charged-Higgs masses, see Fig. 16. Moreover, the existence of multiple SM backgrounds reduces the physics reach for charged Higgs boson discovery at a hadron collider. In contrast, an e^+e^- collider with enhanced charged-scalar pair-production cross-section thanks to the new t-channel contribution and with a considerably cleaner environment is more promising for charged-scalar searches.

7. DECAY MODES OF HEAVY NEUTRINOS AND NEW SCALARS

The decays of the new scalars are controlled by the underlying $U(1)_L$ lepton symmetry. In the limit of very small v_χ , the neutral scalars H and A are almost degenerate in mass. They can be lighter or heavier than the charged Higgs boson, i.e. $m_{A,H} \geq m_{H^\pm}$ for $\lambda_4 \geq 0$ and $m_{A,H} \leq m_{H^\pm}$ for $\lambda_4 \leq 0$. The new scalar masses can also be smaller or larger than the mass of heavy neutrinos. Let us now discuss the decay modes of the H/A , H^\pm scalars as well as the heavy neutrino mediators.

7.1. Decay modes of heavy neutrinos N

The general structure of the weak interactions of the heavy neutrino mass mediators N_i in seesaw models is well-known [6, 12]. The heavy neutrinos can decay into various final states depending on their mass M_{N_i} via their mixing with light neutrinos present in the SM charged and neutral currents.

For $M_{N_i} < m_W$ these are 3-body decays, either purely leptonic $N_i \rightarrow \ell_1 \ell_2 \nu$, 3ν or semileptonic, such as $\ell_1 u \bar{d}$ and $\nu_{\ell_1} q \bar{q}$. The analytical expressions for these decay widths can be found in Ref. [89, 97]. On the other hand, for relatively large M_{N_i} , two-body decay channels such as ℓW , $\nu_\ell Z$ and $\nu_\ell h$ start to dominate.

In the left panel we show the heavy neutrino decay length as a function of its mass and light-heavy neutrino mixing angle. The white triangular region is excluded from electroweak precision data (EWPD-e) [98, 99]. Note that the discontinuity in L_N is due to the jump of the Γ_N around $M_{N_i} \sim 80$ GeV which comes from the threshold of gauge boson masses $M_{W,Z}$. We see that for sufficiently small mixing and relatively small M_{N_i} , the heavy neutrinos are long-lived particles that can travel macroscopic distances before they decay, giving rise to displaced vertex signatures. However, for $M_{N_i} > 50$ GeV and $|V_{eN_i}|^2 > 10^{-8}$, the heavy-

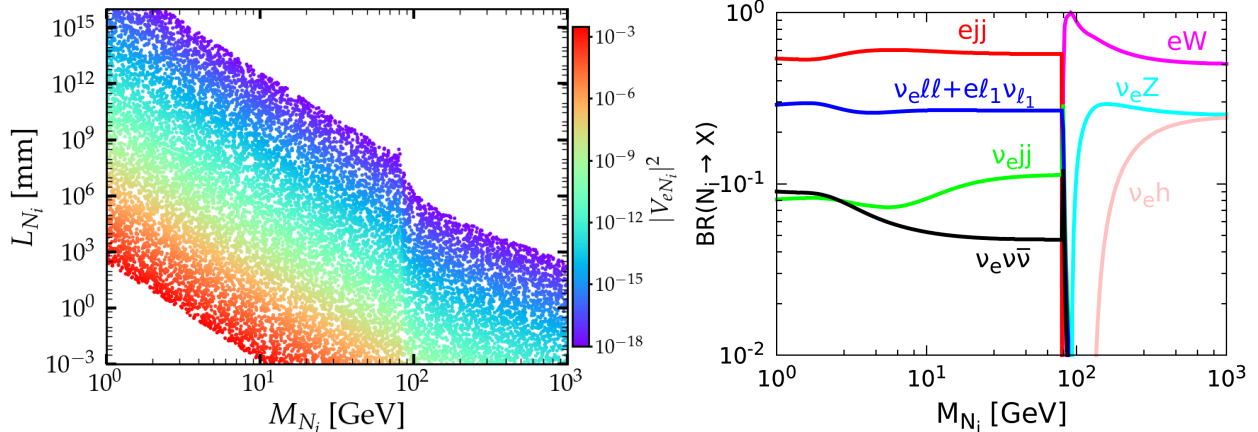


FIG. 19: Left panel: The heavy neutrino decay length as a function of its mass for different values of the light-heavy mixing parameter V_{eN_i} . Right panel: Branching ratios of N_i to various SM final states under the assumption $V_{eN_i} \neq 0$, $V_{\mu N_i} = 0$ and $V_{\tau N_i} = 0$.

neutrino decay-length is quite small, so we can take the heavy-neutrino decay as prompt in most of the parameter space.

In the right panel of Fig. 19, we show the branching ratios (BR) of heavy neutrinos N_i to various final states. For simplicity we took $V_{eN_i} \neq 0$, $V_{\mu N_i} = 0$ and $V_{\tau N_i} = 0$, and assumed that the mixing angle is large enough so that the decay is prompt. With our assumption that the heavy neutrino only mixes with one lepton generation, the branching ratio does not depend on neutrino mixing and the heavy neutrino can decay to one, two or three lepton final states. For relatively small M_{N_i} three-body decays dominate, specially ℓjj . Once the heavy neutrino mass cross the W , Z and h mass thresholds, it starts to decay dominantly to two-body final states. Indeed, Fig. 19 shows that for large M_{N_i} two-body decay such as eW , $\nu_e Z$ and $\nu_e h$ dominate.

Note that in our model, as long as the lepton number violation VEV v_χ is very small, the Yukawa coupling Y_S can be large and still be consistent with neutrino mass. One sees that, as long as $M_{N_i} > m_{H^\pm}, m_{H/A}$, the following decay channels will dominate over decay channels coming from light-heavy neutrino mixing:

$$\Gamma(N_i \rightarrow \ell^\pm H^\mp) \approx \frac{|(Y_S)_{\ell i}|^2 \sin^2 \beta}{32\pi} M_{N_i} \left(1 - \frac{m_{H^\pm}^2}{M_{N_i}^2}\right)^2, \quad (64)$$

$$\Gamma(N_i \rightarrow \nu_\ell H) \approx \frac{|(Y_S)_{\ell i}|^2 \cos^2 \alpha}{64\pi} M_{N_i} \left(1 - \frac{m_H^2}{M_{N_i}^2}\right)^2, \quad (65)$$

$$\Gamma(N_i \rightarrow \nu_\ell A) \approx \frac{|(Y_S)_{\ell i}|^2 \sin^2 \beta}{64\pi} M_{N_i} \left(1 - \frac{m_A^2}{M_{N_i}^2}\right)^2, \quad (66)$$

for large Y_S and neglecting the lepton masses.

In Fig. 20, we show the total decay width of N_i for $M_{N_i} > m_{H^\pm}, m_{H/A}$. One can see that,

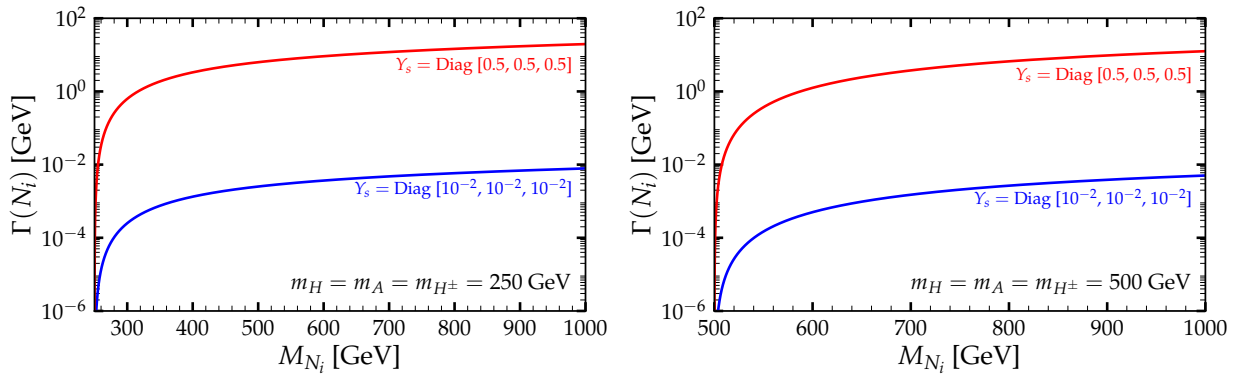


FIG. 20: Total N_i decay width versus its mass for different Y_S and scalar mass values. The left and right panels are for $m_{H/A, H^\pm} = 250$ GeV and $m_{H/A, H^\pm} = 500$ GeV, respectively. The blue and red lines correspond to different Yukawa coupling values Y_S , as indicated.

for larger Y_S values, the decay width is much larger than that coming just from light-heavy mixing and, as expected, increases as M_{N_i} increases. One sees that, as long as masses are far enough from the edge of phase space, 250 GeV and 500 GeV in our case, there is no substantial effect on the decay width. Moreover, even for relatively small $Y_S \sim \mathcal{O}(10^{-2})$, the decay width is always large enough such that N_i is not long-lived. In this case, its branching ratios obey the following relations:

$$\text{BR}(N_i \rightarrow \ell^\pm H^\mp) : \text{BR}(N_i \rightarrow \nu_\ell H) : \text{BR}(N_i \rightarrow \nu_\ell A) = 2 : 1 : 1. \quad (67)$$

Note that for smaller mass of N_i , one can have decay modes such as $\ell_i^\pm qq'$, $\ell_i^\pm \ell_j^\mp \nu$ and $\nu_\ell \nu \bar{\nu}$ through the off-shell decay of $H^\pm, H/A$. However in our range of interest for v_χ , the contribution of new scalars to these 3-body decay modes will be negligible compared to the contribution coming from SM gauge boson exchange involving light-heavy neutrino mixing. This feature is apparent in the small variation of the N_i decay width with changing masses of the scalars. This follows from the leptophilic nature of the new scalars, for example, their couplings to quarks $q'qH^\pm, qqH, qqA$ are all suppressed as $\mathcal{O}(\frac{v_\chi}{v})$. We will discuss this further in the next section.

7.2. H/A and H^\pm decay modes

We now turn to the decays of the new scalar particles, which are basically determined by the $U(1)_L$ symmetry. The decay pattern of new scalars will also depend on whether these are heavier or lighter than heavy neutrinos N_i . For example, Fig. 21 shows the branching ratios of H, A and H^\pm to various decay channels as a function of v_χ assuming $m_{H/A, H^\pm} < M_{N_i}$. Hence as long as v_χ is small, in this kinematical regime the dominant decay modes are $H/A \rightarrow \nu\nu$ and $H^\pm \rightarrow \ell^\pm \nu$. Since in our model the new neutral and charged scalars H/A and H^\pm

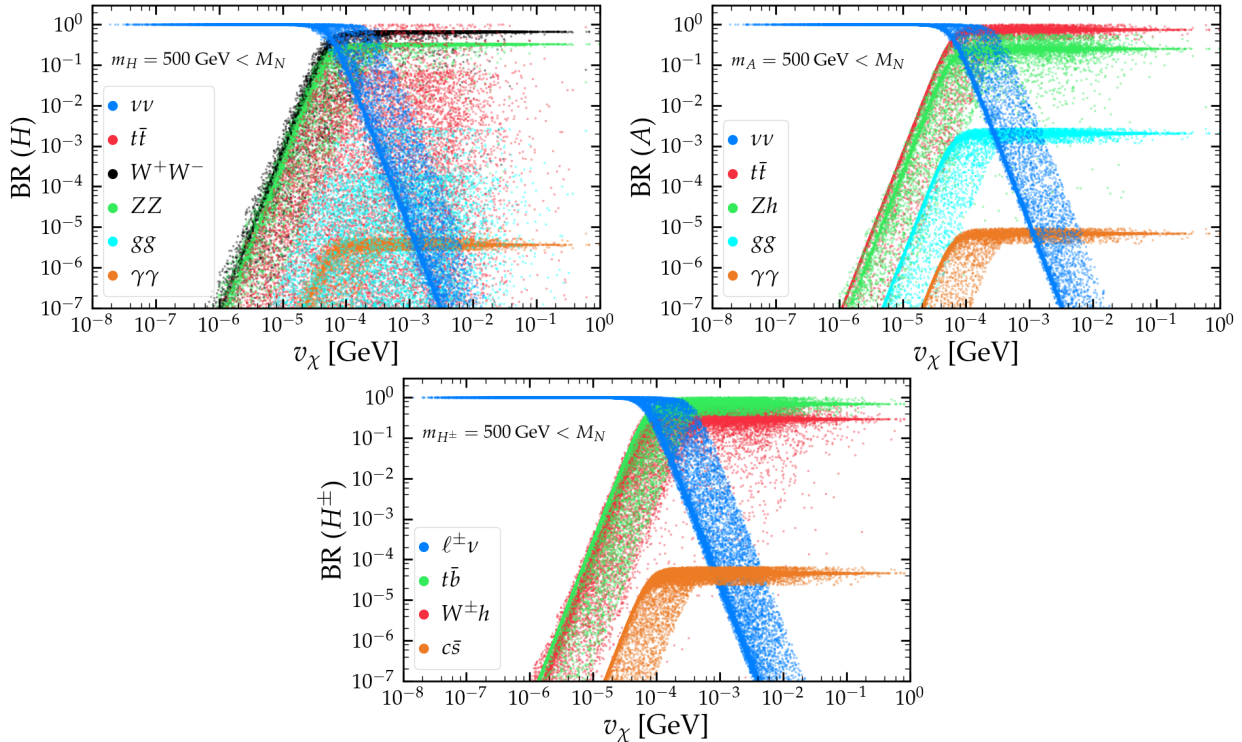


FIG. 21: Neutral and charged Higgs boson decay branching ratios versus v_χ for $m_{H,A,H^\pm} = 500\text{GeV} < M_{N_i}$ and M_{N_i} randomly varied from 1 TeV to 100 TeV.

are mainly composed by χ_L with just a tiny admixture of Φ , couplings such as $(H/A)WW$, $(H/A)ZZ$, $(H/A)\ell\ell$, $(H/A)qq$, AhZ , $H^\pm qq'$ and $H^\pm W^\mp h$ are all suppressed by $\mathcal{O}(v_\chi/v)$. It follows that for small values of v_χ the $H/A \rightarrow \nu\nu$ and $H^\pm \rightarrow l^\pm\nu$ decay channels dominate. On the other hand, Fig. 21 shows that other channels such as $H/A \rightarrow qq$, $H^\pm \rightarrow qq'$ or H/A or H^\pm decaying to the SM gauge bosons dominate over the $H/A \rightarrow \nu\nu$ or $H^\pm \rightarrow l^\pm\nu$ channels if v_χ is relatively large. Similar results follow for the case of $m_{A/H,H^\pm} > M_N$. In this case for small v_χ , the dominant decay modes are $H/A \rightarrow \nu N$ and $H^\pm \rightarrow \ell^\pm N$.

Hence, in our range of interest for v_χ , the relevant decay modes are either $H/A \rightarrow \nu\nu$, $H^\pm \rightarrow \ell^\pm\nu$ ($m_{A/H,H^\pm} < M_N$) or $H/A \rightarrow \nu N$, $H^\pm \rightarrow \ell^\pm N$ ($m_{A/H,H^\pm} > M_N$). In the following subsection we discuss in detail the expressions of these relevant decay widths and how they depend on the model parameters.

1. $m_{H/A}, m_{H^\pm} < M_{N_i}$

In this scenario for very small values of v_χ , or $\alpha \approx 0, \beta \approx \frac{\pi}{2}$, the charged Higgs boson dominantly decays to light neutrinos and charged leptons via the Yukawa interaction. The

decay width is

$$\Gamma(H^\pm \rightarrow \ell^\pm \nu_i) \approx \frac{|(Y_S M_N^{-1} Y_\nu^\dagger)_{\ell i}|^2 v^2 \sin^4 \beta}{32\pi} m_{H^\pm}. \quad (68)$$

On the other hand neutral scalars H/A for small values of v_χ dominantly decay to light neutrinos:

$$\Gamma(H \rightarrow \nu_i \nu_j) \approx \frac{|(Y_S M_N^{-1} Y_\nu^\dagger)_{ij}|^2 v^2 \cos^2 \alpha \sin^2 \beta}{64\pi} m_H, \quad (69)$$

$$\Gamma(A \rightarrow \nu_i \nu_j) \approx \frac{|(Y_S M_N^{-1} Y_\nu^\dagger)_{ij}|^2 v^2 \sin^4 \beta}{64\pi} m_A. \quad (70)$$

Hence, in the limit of very small v_χ , the decay width of H^\pm , H/A will be strongly suppressed for small values of Y_S or for heavy neutrino mass and therefore, these particles can be long-lived. On the other hand, for relatively large v_χ , the Yukawa coupling Y_ν is small if $Y_S \neq 0$ implying that decay modes such as $H^\pm \rightarrow \ell^\pm \nu$ and $H/A \rightarrow \nu\nu$ will again be suppressed. However, the scalars will not necessarily be long-lived as with relatively large v_χ , the small mixing in the scalar sector becomes crucial. In this scenario, charged and neutral Higgs will dominantly decay into quarks or gauge bosons. The expressions for these decay widths are given in Appendix A.

Fig. 21 shows the branching ratios of H , A and H^\pm to various decay channels as a function of v_χ assuming $m_{H,A,H^\pm} < M_{N_i}$. For these plots, we have scanned the parameter space according to Table. II. We have ensured vacuum stability and perturbativity of the λ parameters. We have also taken into account neutrino oscillation data in varying the Yukawas Y_ν , Y_S , imposing also the perturbative requirements $\text{Tr}(Y_\nu^\dagger Y_\nu) < 4\pi$, $\text{Tr}(Y_S^\dagger Y_S) < 4\pi$. One can see that for small values of v_χ , the $H \rightarrow \nu\nu$, $A \rightarrow \nu\nu$ and $H^\pm \rightarrow l^\pm \nu$ decay channels dominate over all other channels. This is easy to understand since in this case the Yukawa coupling Y_ν can be relatively large. For large values of v_χ , as the Yukawa coupling Y_ν needs to be small, other channels involving scalar mixing (particularly the $H \rightarrow VV$, $A \rightarrow q\bar{q}$, $A \rightarrow hZ$ and $H^\pm \rightarrow t\bar{b}$, $H^\pm \rightarrow W^\pm h$ channels) dominate over the $H/A \rightarrow \nu\nu$ and $H^\pm \rightarrow l^\pm \nu$ channels.

2. $m_{H/A}, m_{H^\pm} > M_{N_i}$

In the complementary case where $m_{H/A}, m_{H^\pm} > M_{N_i}$, the charged Higgs bosons dominantly decay through the Yukawa interaction into charged leptons ℓ^\pm and on-shell heavy neutrinos N_i as

$$\Gamma(H^\pm \rightarrow \ell^\pm N_i) \approx \frac{|(Y_S)_{\ell i}|^2 \sin^2 \beta}{16\pi} m_{H^\pm} \left(1 - \frac{M_{N_i}^2}{m_{H^\pm}^2}\right)^2, \quad (71)$$

whereas the neutral Higgs bosons dominantly decay into light neutrinos ν_ℓ and on-shell heavy neutrinos N_i as

$$\Gamma(H \rightarrow \nu_\ell N_i) \approx \frac{|(Y_S)_{\ell i}|^2 \cos^2 \alpha}{32\pi} m_H \left(1 - \frac{M_{N_i}^2}{m_H^2}\right)^2 \quad (72)$$

$$\Gamma(A \rightarrow \nu_\ell N_i) \approx \frac{|(Y_S)_{\ell i}|^2 \sin^2 \beta}{32\pi} m_A \left(1 - \frac{M_{N_i}^2}{m_A^2}\right)^2. \quad (73)$$

Note that in the limit of small v_χ , the dominant decay modes in this case are proportional to Y_S^2 . Therefore, in contrast to the previous case, within the linear seesaw the decays are not suppressed by heavy-neutrino mass beyond the phase-space factor, as the Yukawa coupling Y_S can be large even for weak-scale mediators consistent with neutrino mass. It follows that the scalars will not be long-lived even for small v_χ . As in the previous case, for Y_S small or v_χ relatively large, the small mixing in the scalar sector becomes important and the charged and neutral Higgs scalars will dominantly decay into quarks or gauge bosons. The expressions for these decay widths are given in Appendix A.

8. COLLIDER SIGNATURES

Having discussed the various heavy-neutrino-mediator and new scalar production modes, we now discuss the associated collider signatures. Once the heavy neutrinos or new scalars are produced, they will further decay to various possible decay channels depending on kinematical considerations. For example, if $M_{N_i} > m_{H^\pm}, m_{H/A}$ and Y_S is large, heavy neutrinos will dominantly decay to final states such as $\ell^\pm H^\mp$ and $\nu_\ell H/A$. On the other hand, if $M_{N_i} < m_{H^\pm}, m_{H/A}$, heavy neutrinos will decay to SM final states such as ℓW , νZ and νh through light-heavy neutrino mixing. Let us now discuss the possible signatures associated to various production processes:

$$\underline{e^+e^- \rightarrow N_i N_i}$$

In Fig. 22, we show the various possible final states coming from the pair production of heavy neutrinos at e^+e^- collider. The first row of Fig. 22 corresponds to the case of $M_{N_i} < m_{H^\pm}$, whereas the second row is for the case of $m_{N_i} > m_{H^\pm}$. When $M_{N_i} < m_{H^\pm}$, N_i will dominantly decay to SM final states through light-heavy neutrino mixing and we depict the charged-current-mediated decay mode $N_i \rightarrow \ell W$ with W boson decaying leptonically or hadronically.

If both W boson decays hadronically, we have lepton number violating (LNV) and lepton number conserving (LNC) final states $\ell_i^\pm \ell_i^\pm 4j$ and $\ell_i^\pm \ell_i^\mp 4j$, respectively. When the decay width Γ_N is comparable or smaller than the mass splitting within the quasi-Dirac pair

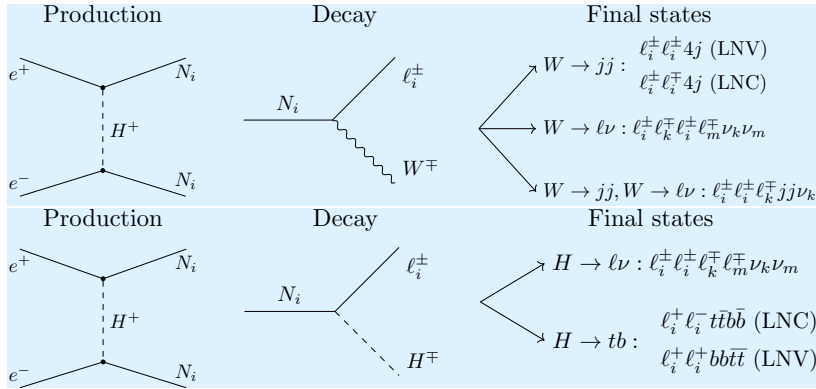


FIG. 22: Illustrative representation of heavy-neutrino pair-production and decay channels. The upper row is for the case of $M_{N_i} < m_{H^\pm}$ and the bottom one is for $M_{N_i} > m_{H^\pm}$.

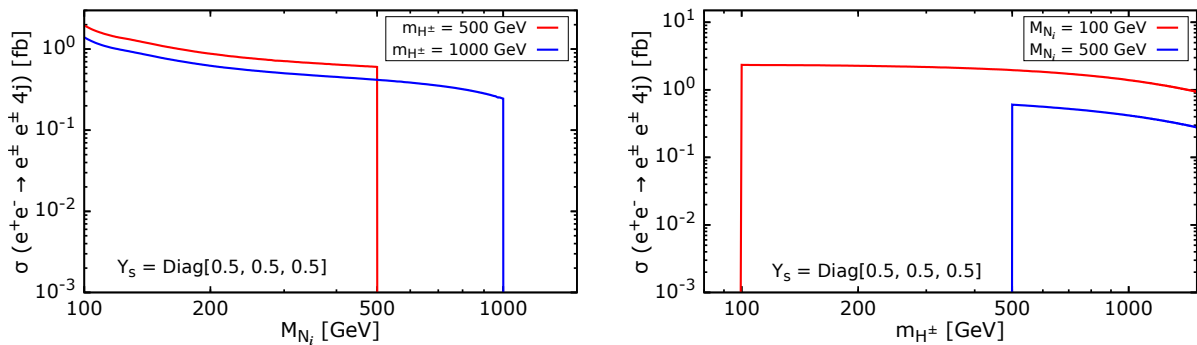


FIG. 23: Cross-section for the process $e^+e^- \rightarrow N_i N_i \rightarrow e^\pm e^\pm 4j$ versus the mass of heavy neutrinos M_{N_i} (left panel), and versus the mass of charged Higgs m_{H^\pm} (right panel).

$\Delta M \sim m_\nu$, the cross section for both the LNV and LNC final states can be of the same order, see Appendix B for a detailed discussion. The LNV same-sign dilepton final state is quite interesting as it may help probing the Majorana nature of neutrinos [74]. Moreover, the LNV signal $\ell_i^\pm \ell_i^\pm 4j$ is almost free of SM backgrounds.

In Fig. 23, we show the cross section for the process $e^+e^- \rightarrow N_i N_i \rightarrow e^\pm e^\pm 4j$ at $\sqrt{s} = 3$ TeV under the assumption $|V_{eN_i}| \neq 0$, $|V_{\mu N_i}| = |V_{\tau N_i}| = 0$. The left and right panel stands for the cross-section with respect to M_{N_i} and m_{H^\pm} where we fix the Yukawa coupling $Y_s = \text{Diag}(0.5, 0.5, 0.5)$. Different lines in each panel correspond to different values of charged Higgs or heavy neutrino mass.

If both the W bosons decay leptonically, we will have multileptonic final states associated with missing transverse energy such as $\ell_i^\pm \ell_i^\pm \ell_k^\mp \ell_m^\mp + \cancel{E}_T$. On the other hand, if one of the W bosons decays leptonically and other one decays hadronically, we can have semileptonic final states in association with missing transverse energy such as $\ell_i^\pm \ell_i^\pm \ell_k^\mp jj + \cancel{E}_T$. Such final states will have large enough cross-sections, as the leptonic branching ratio $\text{BR}(W \rightarrow \ell\nu)$ is almost 10% while the hadronic branching ratio is $\text{BR}(W \rightarrow jj) \approx 67\%$. However, unlike the

LNV final states, for these final states there will be SM backgrounds, requiring a dedicated analysis in order to reduce them.

The lower diagrams in Fig. 22 show the other final states possible for the case of $M_{N_i} > m_{H^\pm}, m_{H/A}$. In this case N_i will dominantly decay to $\ell^\pm H^\mp$ or $\nu H/A$. Here we only show the possible final states coming from the decay chain $N_i \rightarrow \ell^\pm H^\mp$ and $H^\pm \rightarrow \ell^\pm \nu$ or $H^\pm \rightarrow tb$. As seen in Fig. 21, when v_χ is very small the dominant decay mode is $H^\pm \rightarrow \ell^\pm \nu$, while for relatively large v_χ , the dominant mode is $H^\pm \rightarrow tb$. Although in the small v_χ limit $H^\pm \rightarrow \ell^\pm \nu$ is the dominant decay mode, the decay width can be strongly suppressed for small values of Y_S or for very heavy neutrino masses. In this case H^\pm can be long-lived and hence the secondary charged tracks of the long-lived charged Higgs boson can be tagged at the ILC. However, if Y_S is relatively large or M_{N_i} is not so large, then H^\pm will not be long-lived and H^\pm to $\ell^\pm \nu$ can give rise to multilepton final states containing missing energy, i.e. $\ell_i^\pm \ell_i^\pm \ell_k^\mp \ell_m^\mp + \cancel{E}_T$. The cross-section for this final state is of the same order as for the LNV same-sign dilepton final state shown in Fig. 23. On the other hand, for relatively large v_χ , the decay chain $H^\pm \rightarrow tb$ will give rise to both LNV and LNC final states such as $\ell_i^+ \ell_i^+ b\bar{t}\bar{t}$ and $\ell_i^+ \ell_i^- t\bar{t}b\bar{b}$, respectively. However, these are suppressed in the small v_χ limit.

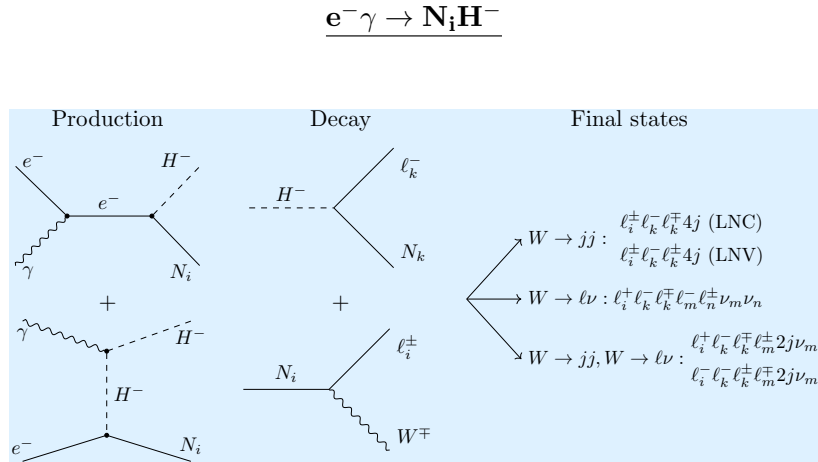


FIG. 24: Illustrative representation of the heavy neutrino production in association with charged Higgs and the expected decay channels for the case $M_{N_i} < m_{H^\pm}$.

In Fig. 24 we show the possible interesting final states coming from the process $e^- \gamma \rightarrow N_i H^-$ when $m_{H^\pm} > M_{N_i}$. A possible decay chain is $H^\pm \rightarrow \ell_i^\pm N_i$, with $N_i \rightarrow \ell_i^\pm W^\mp$, and either leptonic or hadronic decay of the W boson. If both W bosons decay hadronically, one can have LNV or LNC trilepton final state such as $\ell_i^\pm \ell_k^- \ell_k^\pm 4j$ and $\ell_i^\pm \ell_k^- \ell_k^\mp 4j$, respectively. Again, the LNV signal $\ell_i^\pm \ell_k^- \ell_k^\pm 4j$ seems more interesting, as it is free from the SM background and might help probing the Majorana nature of neutrinos [74]. In Fig. 25 we show the cross section for the LNV final state $e^\pm e^- e^\pm 4j$ at $\sqrt{s} = 3$ TeV assuming $|V_{eN_i}| \neq 0$, $|V_{\mu N_i}| = |V_{\tau N_i}| = 0$. The left and right panels show the cross-section versus M_{N_i} and m_{H^\pm} fixing

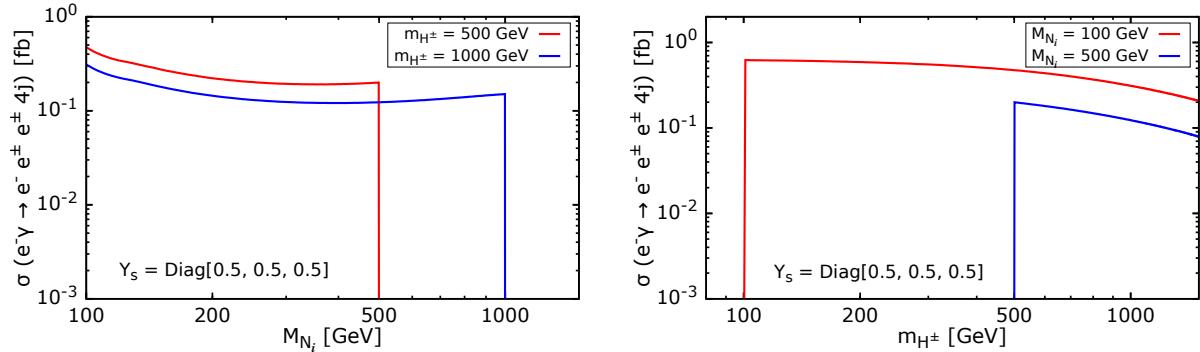


FIG. 25: Cross-section for the process $e^- \gamma \rightarrow H^- N_i \rightarrow e^- e^\pm e^\pm 4j$ versus the heavy-neutrino mediator mass M_{N_i} (left panel), and versus the charged Higgs mass m_{H^\pm} (right panel).

the Yukawa coupling as $Y_S = \text{Diag}(0.5, 0.5, 0.5)$. Different lines in each panel correspond to different values of the charged Higgs or heavy neutrino masses. Similar to the previous case, if both the W bosons decay leptonically, or if one W decays hadronically and other one leptonically, we will have pure multileptonic or semi-leptonic final states, respectively, accompanied by missing energy.

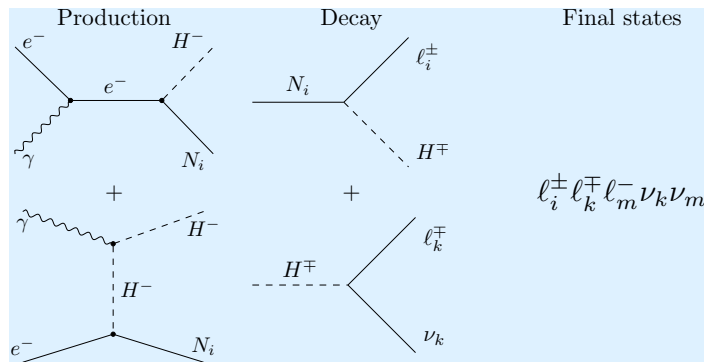


FIG. 26: Illustrative representation of the heavy neutrino production in association with charged Higgs and their various decay channels for the case of $M_{N_i} > m_{H^\pm}$.

Fig. 26 shows the possible final states arising from the process $e^- \gamma \rightarrow N_i H^-$ for the case when $M_{N_i} > m_{H^\pm}$ and Y_S is large. This case seems not too interesting phenomenologically, as the final states have large missing energy. Other decay modes of H^\pm for the $M_{N_i} > m_{H^\pm}$ case are small for small ν_χ , hence are not discussed here.

$$\underline{e^+ e^- / pp} \rightarrow \underline{H^+ H^-}$$

In Fig. 27, we show interesting final states coming from the production process $e^+ e^- / pp \rightarrow H^+ H^-$ when $m_{H^\pm} > M_{N_i}$. Note that at a pp collider production comes only through the Drell-Yan mechanism, whereas for large Y_S the production at lepton colliders is dominated by

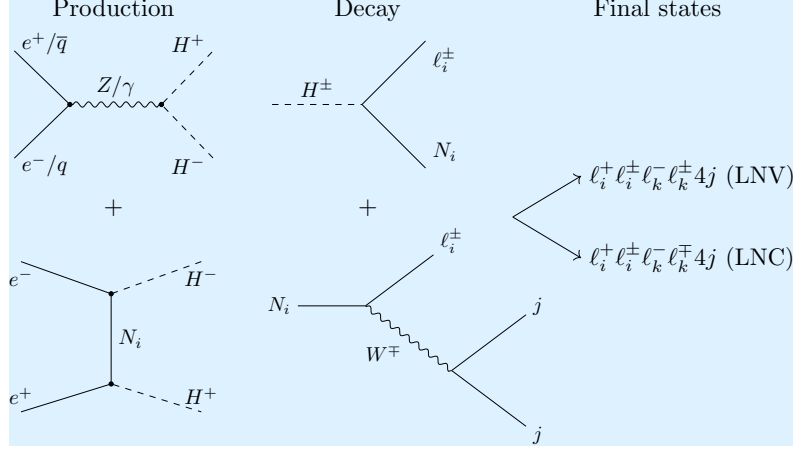


FIG. 27: Illustrative representation of the pair of charged Higgs production and the expected decay channels for the case $M_{N_i} < m_{H^\pm}$.

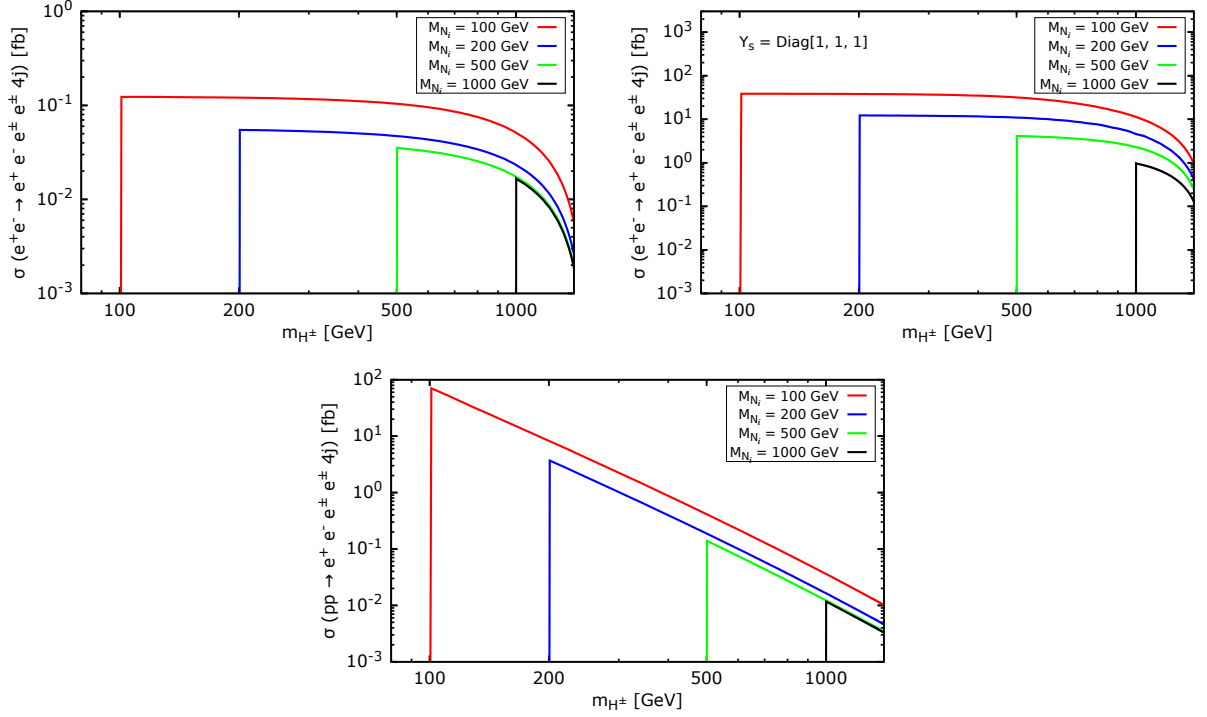


FIG. 28: Cross-section for the process $XX \rightarrow H^+H^- \rightarrow e^+N_i e^-N_i \rightarrow e^+e^-e^\pm 4j$ versus the charged scalar mass. For the upper left panel we have taken only the s-channel contribution to the process $e^+e^- \rightarrow H^+H^-$ whereas for the upper right panel we took both the s- and the t-channel contributions for $Y_s = \text{Diag}(1, 1, 1)$. We took the center of mass energies $\sqrt{s} = 3$ TeV and $\sqrt{s} = 100$ TeV for the e^+e^- collider and pp collider, respectively.

the t-channel heavy neutrino mediation. From the decay chain $H^\pm \rightarrow \ell_i^\pm N_i$, $N_i \rightarrow \ell_i^\pm W^\mp$, $W \rightarrow jj$, we find two very interesting semileptonic final states: $\ell_i^+ \ell_i^\pm \ell_k^- \ell_k^\pm 4j$ (LNV) and $\ell_i^+ \ell_i^\pm \ell_k^- \ell_k^\mp 4j$ (LNC). In Fig. 28 we show the cross section for the LNV final state $XX \rightarrow e^+e^\pm e^-e^\pm 4j$ under the assumption $|V_{eN_i}| \neq 0$, $|V_{\mu N_i}| = |V_{\tau N_i}| = 0$. Different lines in each

panel correspond to different values of the heavy neutrino masses. The upper panel is for $\sqrt{s} = 3$ TeV e^+e^- collider where in the left panel we only take into account the contribution coming from the Drell-Yan mechanism while in the right panel we include both the Drell-Yan and the t-channel contribution with Yukawa coupling $Y_S = \text{Diag}(1, 1, 1)$. Comparing the left and right panels of Fig. 28 one sees that there is a huge enhancement in the production rate once we take into account the t-channel contribution. In the bottom panel of Fig. 28 we show the LNV cross-section at a proton-proton collider with $\sqrt{s} = 100$ TeV. Note that the specific Yukawa coupling values do not matter for the case of hadron collider, as the cross-section comes just from the Drell-Yan contribution. Therefore, the pair production cross-section of charged scalars at hadron collider becomes smaller for large charged Higgs masses.

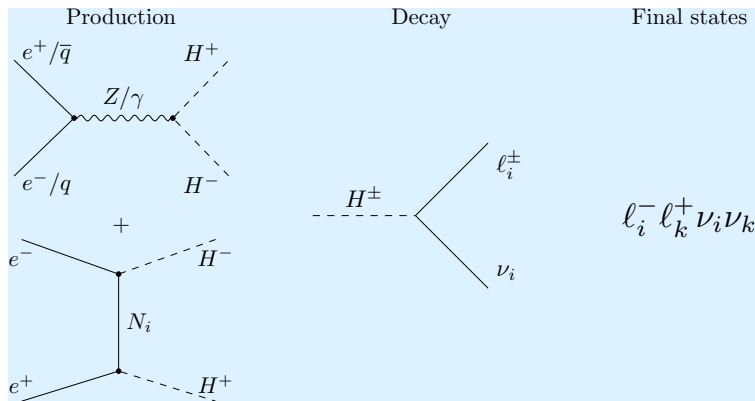


FIG. 29: Illustrative representation of the charged-Higgs pair-production and their various decay channels for the case of $M_{N_i} > m_{H^\pm}$.

Fig. 29 shows the possible final states coming from $pp \rightarrow H^+H^-$ or $e^+e^- \rightarrow H^+H^-$ for $M_{N_i} > m_{H^\pm}$ case. For small v_χ values, H^\pm dominantly decays to $\ell^\pm\nu$, which leads to the large missing energies in the final states. H^\pm can decay to heavy quarks, tb , but this channel is $\mathcal{O}(v_\chi/v)$ suppressed. Altogether, the phenomenology for the $M_{N_i} > m_{H^\pm}$ case seems not too interesting.

Note that in all of our above discussion of collider signatures, we have considered the heavy neutrinos decay through the charged current interaction. One can also consider scenarios where both heavy neutrinos decay through neutral current interaction, such as $N \rightarrow \nu Z$ or a scenario where one of them decays as $N \rightarrow \ell W$ and other one decay as $N \rightarrow \nu Z$. Taking into account the Z boson leptonic decay mode, and the leptonic/hadronic decay modes of the W boson, one finds many interesting final states with high lepton multiplicity, as listed in Appendix C.

9. CONCLUSIONS

In summary we studied the linear seesaw mechanism where neutrino masses arise from a second scalar doublet χ_L with lepton number $L[\chi_L] = -2$. The model has three pairs of fermion singlets ν_i^c, S_i with lepton number $L[\nu_i^c] = -1$ and $L[S_i] = 1$ as neutrino mass mediators, see Fig. 1. The smallness of neutrino mass is dynamically explained by the tiny induced VEV of the new Higgs doublet χ_L . The scenario provides an attractive benchmark for collider physics, in which the new scalar Higgs bosons $H^\pm, H/A$ as well as the heavy neutrinos can be kinematically accessible.

We have discussed existing restrictions from neutrino masses and electroweak precision data, that leads to a compressed scalar boson spectrum, see Fig. 2. One sees from Fig. 8 that LHC searches for rare $\gamma\gamma$ Higgs boson decays do not place any important restrictions on the charged Higgs mass in Fig. 7. Moreover, we have investigated the novel features associated to cLFV, see Figs. 5 and 6. Apart from the charged current contribution involving heavy or light neutrinos, there are also charged Higgs contributions to the cLFV rates coming from the Yukawa interactions in the right panel of Fig. 3.

Note that the scale of the new fermions mediating neutrino mass generation can lie at the TeV scale and may be accessible at various collider setups. As a consequence, our linear seesaw mechanism offers a very intriguing alternative to the classic high-scale type-I seesaw mechanism. Indeed, the fact that the Yukawa couplings Y_ν and Y_S can be sizeable makes our model testable at collider experiments. We find that unlike the simplest type-I seesaw mechanism, our proposal offers new unsuppressed heavy-neutrino production mechanisms at various colliders. For example, as illustrated in Figs. 10, 11 and Figs. 12, 13, 14, the heavy neutrinos can be produced at e^+e^- and $e^-\gamma$ colliders through charged-Higgs boson exchange. These production rates are proportional to Y_S^4 , and hence can be sizeable while consistent with smallness of neutrino masses, since the latter can be ascribed to the small value of v_χ .

We looked at the production of new scalars in pp as well as the e^-e^+ colliders as shown in Figs. 15, 16, 17 and 18. Specifically we found that $e^+e^- \rightarrow NN$ and $e^-\gamma \rightarrow NH^-$ followed by $H^\pm \rightarrow \ell^\pm N$ decay provides a promising way to produce heavy neutrinos. Moreover, besides the usual Drell-Yan mechanism in e^+e^- collisions, one can have heavy-neutrino-mediated charged-Higgs boson pair production $e^+e^- \rightarrow H^\pm H^\mp$ as shown in Figs. 17 and 18. The latter can dominate over Drell-Yan production for large Yukawa coupling Y_S .

Once the charged-Higgs bosons are produced, the heavy seesaw mediator neutrinos will be produced in their decays, $H^\pm \rightarrow \ell^\pm N$, effectively enhancing the heavy neutrino production rates. Moreover, assuming $m_{H^\pm, H/A} > M_{N_i}$, the produced heavy neutrinos dominantly decay to SM final states such as $\ell W, \nu Z$ and νh through the light-heavy neutrino mixing. We find that the decay chain $N_i \rightarrow \ell_j^\pm W^\mp$ with $W^\mp \rightarrow jj$ leads to interesting collider signatures.

Fig. 19 shows the decay length and branching fractions of the heavy neutrinos due to the light-heavy neutrino mixing, while Fig. 20 displays the decay widths of the heavy neutrinos when $M_{N_i} > m_{H/A/H^\pm}$. In this case, the scalars decay to various SM final states as shown in Fig. 21. For the case $m_{H/A/H^\pm} > M_{N_i}$, the scalars dominantly decay into heavy neutrinos and SM leptons. The production and decay of the heavy neutrinos at e^+e^- collider as illustrated in Fig. 22, leads to lepton number conserving as well as violating final states. The cross-section for LNV/LNC final states $e^\pm e^\pm 4j / e^\pm e^\mp 4j$ at e^+e^- colliders is shown in Fig. 23.

Moreover, we also discussed the decays of charged-Higgs and heavy-neutrinos at $e^- \gamma$ colliders, as shown in Fig. 24. In Fig. 25 we display the cross-section for the resulting three-lepton-four-jet final states $e^- e^\pm e^\pm 4j / e^- e^\pm e^\mp 4j$. Likewise the production and decay of charged scalars can also lead to four-lepton-four-jet final states $e^+ e^- e^\pm e^\pm 4j / e^+ e^- e^\pm e^\mp 4j$ as depicted in Fig. 27. In Fig. 28 we show the associated cross-sections at pp and e^-e^+ colliders for the production of various LNV/LNC high multiplicity final states $e^+e^- e^\pm e^\pm 4j / e^+e^- e^\pm e^\mp 4j$.

We also stress that some of the above signatures involve lepton number violating final states, hence their possible detection would provide an indirect test of the Majorana nature of neutrinos, complementary to that provided by neutrinoless double beta decay searches.

Last, but not least, note that the discussion presented in our paper can be easily extended to the proposed muon collider [100, 101]. In this case too one expects a plethora of interesting signatures arising from our leptophilic Higgs portal.

Acknowledgments

The work of A.B. is supported by Fundação para a Ciência e a Tecnologia (FCT, Portugal) through the PhD grant UI/BD/154391/2023 and through the projects CFTP-FCT Unit UIDB/00777/2020 and UIDP/00777/2020, CERN/FIS-PAR/0019/2021, which are partially funded through POCTI (FEDER), COMPETE, QREN and EU. The work of P.B. is supported by the CSIR JRF-NET fellowship. The work of S.M. is supported by KIAS Individual Grants (PG086001) at Korea Institute for Advanced Study. The work of RS is supported by the Government of India, SERB Startup Grant SRG/2020/002303. The work of J.V. is supported by the Spanish grants PID2020-113775GB-I00 (AEI/10.13039/501100011033) and Prometeo CIPROM/2021/054 (Generalitat Valenciana).

Appendix A: Scalar Decay Width Expressions

Here we discuss the various possible decay modes of the new scalars present in our linear seesaw model, including decay channels to quarks, gauge, as well as Higgs bosons.

1. $H_i \rightarrow f\bar{f}'$

The decay width of the new scalars H , A and H^\pm to fermions are given in equations (A1),(A2) and (A3).

$$\Gamma(H \rightarrow f\bar{f}') = \frac{N_c m_H}{8\pi} \left\{ [1 - (x_1 + x_2)^2] |C_{Hff'}|^2 \right\} \lambda^{1/2}(1, x_1^2, x_2^2), \quad (\text{A1})$$

$$\Gamma(A \rightarrow f\bar{f}') = \frac{N_c m_A}{8\pi} \left\{ [1 - (x_1 - x_2)^2] |C_{Aff'}|^2 \right\} \lambda^{1/2}(1, x_1^2, x_2^2), \quad (\text{A2})$$

$$\Gamma(H^\pm \rightarrow f\bar{f}') = \frac{N_c m_{H^\pm}}{8\pi} \left\{ [1 - (x_1 + x_2)^2] |C_S|^2 + [1 - (x_1 - x_2)^2] |C_P|^2 \right\} \lambda^{1/2}(1, x_1^2, x_2^2) \quad (\text{A3})$$

where $x_1 = m_f/m_{H_i}$, $x_2 = m_{\bar{f}'}/m_{H_i}$, $C_{Hff'} = \sin \alpha \frac{m_f}{v}$, $C_{Aff'} = \cos \beta \frac{m_f}{v}$ and

$$\lambda(1, x, y) = (1 - x - y)^2 - 4xy, \quad (\text{A4})$$

For the physical electrically charged Higgs boson $H^\pm \rightarrow u_i \bar{d}_j$ we have defined

$$C_S = \frac{1}{\sqrt{2}v} (-m_{d_j} + m_{u_i}) V_{\text{CKM}}^{ij} \cos \beta$$

$$C_P = \frac{1}{\sqrt{2}v} (m_{d_j} + m_{u_i}) V_{\text{CKM}}^{ij} \cos \beta$$

here $i, j = 1, 2, 3$.

For decays into quarks, the QCD radiative corrections are included as:

$$\Gamma = \Gamma_0 \left[1 + 5.67 \frac{\alpha_s}{\pi} + (35.94 - 1.36n_f) \left(\frac{\alpha_s}{\pi} \right)^2 \right] \quad (\text{A5})$$

where n_f is the number of quark flavours with $m_q < m_{H_i}$.

2. $H_i \rightarrow VV$

Only the new scalar H has a sizeable decay width to two gauge bosons. The expression for this decay width is shown in equation (A6).

$$\Gamma(H \rightarrow VV) = \delta_V \frac{|C_{H_VV}|^2 m_H^3}{128\pi m_V^4} (1 - 4k + 12k^2) \sqrt{1 - 4k}. \quad (\text{A6})$$

where $k = \frac{m_V^2}{m_H^2}$, $\delta_V = 2(1)$ for $V = W (Z)$,

$$C_{HW+W^-} = \frac{1}{2}ig^2v(\cos\alpha\cos\beta + \sin\alpha\sin\beta)$$

$$C_{HZZ} = \frac{1}{2}iv(\cos\alpha\cos\beta + \sin\alpha\sin\beta)(gc_w + g_Ys_w)^2$$

Here $g = e/c_w$ and $g_Y = e/s_w$

3. $H_i \rightarrow VH_j$

The decay of the new scalars to one SM gauge boson and the Higgs boson are given in equations (A7) and (A8).

$$\Gamma(A \rightarrow hZ) = \frac{|C_{AhZ}|^2 m_V^2}{16\pi^2 m_A} \lambda \left(1, \frac{m_A^2}{m_V^2}, \frac{m_{H_j}^2}{m_V^2} \right) \lambda^{1/2} \left(1, \frac{m_V^2}{m_A^2}, \frac{m_{H_j}^2}{m_A^2} \right), \quad (\text{A7})$$

$$\Gamma(H^\pm \rightarrow W^\pm h) = \frac{|C_{H^\pm W^\pm h}|^2 m_{W^\pm}^2}{16\pi^2 m_{H^\pm}} \lambda \left(1, \frac{m_{H^\pm}^2}{m_{W^\pm}^2}, \frac{m_h^2}{m_{W^\pm}^2} \right) \lambda^{1/2} \left(1, \frac{m_{W^\pm}^2}{m_{H^\pm}^2}, \frac{m_h^2}{m_{H^\pm}^2} \right) \quad (\text{A8})$$

Here

$$C_{AhZ} = \frac{1}{2}(\cos\beta\cos\alpha + \sin\alpha\sin\beta)(-gc_w - g_Ys_w)$$

$$C_{H^\pm W^\pm h} = -\frac{i}{2}g(\sin\alpha\sin\beta + \cos\alpha\cos\beta)$$

4. $H_i \rightarrow \gamma\gamma$

The loop-induced decay width of the new neutral scalars H and A to photons are given in equations (A9) and (A10).

$$\Gamma(H \rightarrow \gamma\gamma) = \frac{\alpha^2 M_H^3}{256\pi^3 v^2} |S^\gamma(M_H)|^2, \quad (\text{A9})$$

$$\Gamma(A \rightarrow \gamma\gamma) = \frac{\alpha^2 M_A^3}{256\pi^3 v^2} |P^\gamma(M_A)|^2, \quad (\text{A10})$$

where the loop factors are

$$S^\gamma(M_H) = 2 \sum_f N_c Q_f^2 C_{Hf\bar{f}} \frac{v}{m_f} F_s(\tau_f) - C_{HW+W^-} \frac{v}{2m_W^2} F_1(\tau_W) - C_{HH+H^-} \frac{v}{2m_{H^\pm}^2} F_0(\tau_{H^\pm}) \quad (\text{A11})$$

and

$$P^\gamma(M_A) = 2 \sum_f N_c Q_f^2 C_{Aff}^P \frac{v}{m_f} F_p(\tau_f) \quad (\text{A12})$$

Here $N_c = 3(1)$ for quarks (leptons), and Q_f is the electric charge and

$$C_{HH^+H^-} = -iv(\cos \alpha \cos \beta^3 \lambda_3 + \sin \alpha \sin \beta^3 \lambda_3 + \cos \beta^2 \sin \alpha \sin \beta (2\lambda_1 - \lambda_4) + \cos \alpha \cos \beta \sin \beta^2 (2\lambda_2 - \lambda_4))$$

The functions $F_s(\tau)$, $F_p(\tau)$, $F_0(\tau)$ and $F_1(\tau)$ are given as in equation (A13).

$$\begin{aligned} F_s(\tau) &= \tau^{-1} \left[1 + (1 - \tau^{-1}) f(\tau) \right] & F_p(\tau) &= \frac{f(\tau)}{\tau} \\ F_0(\tau) &= \tau^{-1} \left[\tau^{-1} f(\tau) - 1 \right] & F_1(\tau) &= 2 + 3\tau^{-1} + 3\tau^{-1} (2 - \tau^{-1}) f(\tau) \end{aligned} \quad (\text{A13})$$

where $\tau_f = m_{H_i}^2/4m_f^2$, $\tau_W = m_{H_i}^2/4m_W^2$, $\tau_{H^+} = m_{H_i}^2/4m_{H^+}^2$ and

$$f(\tau) = \begin{cases} \arcsin^2(\sqrt{\tau}) & \tau \leq 1 \\ -\frac{1}{4} \left[\ln \left(\frac{\sqrt{\tau} + \sqrt{\tau-1}}{\sqrt{\tau} - \sqrt{\tau-1}} \right) - i\pi \right]^2 & \tau > 1. \end{cases} \quad (\text{A14})$$

5. $H_i \rightarrow gg$

The loop-induced decay width of the new neutral scalars H and A to gluons are given in equations (A15) and (A16).

$$\Gamma(H \rightarrow gg) = \frac{\alpha_s^2 M_H^3}{32\pi^3 v^2} |S^g(M_H)|^2, \quad (\text{A15})$$

$$\Gamma(A \rightarrow gg) = \frac{\alpha_s^2 M_A^3}{32\pi^3 v^2} |P^g(M_A)|^2, \quad (\text{A16})$$

with the loop factors

$$S^g(M_H) = \sum_q C_{Hq\bar{q}} \frac{v}{m_q} F_s(\tau_q), \quad P^g(M_A) = \sum_q C_{Aq\bar{q}} \frac{v}{m_q} F_p(\tau_q) \quad (\text{A17})$$

Appendix B: LNV versus LNC in Linear seesaw model

1. Linear seesaw with quasi-Dirac heavy neutrinos

Here we discuss the prospects of having large rates for LNV processes. Let's start by recalling that the rates for LNV and LNC processes are predicted to be the same when mediated by heavy Majorana neutrinos. Within the linear seesaw with softly broken lepton

number, LNV processes should be severely suppressed. This follows from the fact that the quasi-Dirac heavy neutrinos can be thought of as two fermions of opposite CP-phase and small Majorana mass-splitting ($\Delta M \sim m_\nu$). This leads to a cancellation between the individual contributions to LNV processes involving virtual heavy-neutrino propagation.

However, at collider energies heavy neutrino mediators can be produced on-shell, so that oscillations can occur between the members of the quasi-Dirac pair. This can prevent the cancellation suppressing LNV signals. This applies to all low-scale seesaw setups, such as the inverse seesaw or our linear seesaw model. Note that the oscillations between the

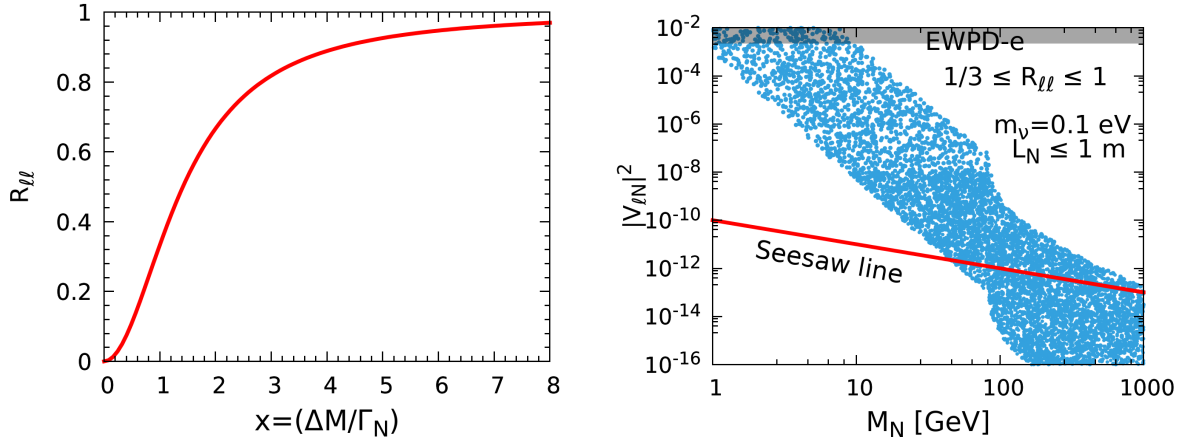


FIG. 30: Left panel: LNV to LNC ratio $R_{\ell\ell}$ versus the quantity $x = \frac{\Delta M}{\Gamma_N}$. Right panel: parameter region in the plane $|V_{\ell N}|^2 - M_N$ for $m_\nu \sim 0.1$ eV yielding $R_{\ell\ell}$ in the range $1/3 \leq R_{\ell\ell} \leq 1$. We also required that the heavy neutrino decay length $L_N < 1$ meter, so that N decays inside the linear collider detector. The gray band is excluded by electroweak precision data, and the red line represents a naive seesaw expectation $|V_{\ell N}|^2 \sim m_\nu/M_N$.

members of quasi-Dirac pair are determined by the mass-splitting ΔM and if $\Delta M \ll \Gamma_N$, they will decay before they have time to oscillate. In this case, the destructive interference between heavy neutrinos will hold and LNV processes are suppressed. On the other hand, if $\Delta M \gg \Gamma_N$, as the heavy neutrinos oscillate many times before they decay, the oscillations are averaged out and the LNV rates are expected to be similar to those of LNC processes. A more dedicated discussion was given in Ref. [55, 102, 103], where it was found that the ratio of the rates for opposite and same-sign dilepton events is effectively characterised by the following expression

$$R_{\ell\ell} = \frac{\Delta M^2}{2\Gamma_N^2 + \Delta M^2} = \frac{x^2}{2 + x^2}, \quad \text{with } x = \frac{\Delta M}{\Gamma_N}. \quad (\text{B1})$$

Note that $R_{\ell\ell} \rightarrow 1$ as $x \rightarrow \infty$ (limiting Majorana case) and $R_{\ell\ell} \rightarrow 0$ as $x \rightarrow 0$ (limiting Dirac case). In models with quasi-Dirac neutrinos, the ratio $R_{\ell\ell}$ can take any value between 0 and 1. In the left panel of Fig. 30 we show $R_{\ell\ell}$ versus $x = \frac{\Delta M}{\Gamma_N}$ for a benchmark value

of the heavy neutrino mass, $M_N = 100$ GeV. We see that when the mass splitting ΔM is larger than a few times the width Γ_N , $R_{\ell\ell}$ approaches rapidly the Majorana limit $R_{\ell\ell} = 1$. Note that this result is independent of the absolute heavy-neutrino mass scale. In our case the mass splitting is $\Delta M \sim m_\nu$ and hence is very tiny. On the other hand the decay width Γ_N is controlled by the mixing parameter $V_{\ell N}$ (when $M_N < m_{H^\pm, H/A}$) or by the Yukawa coupling Y_S ($M_N > m_{H^\pm, H/A}$). In either case the decay width Γ_N is large for relatively large mixing $V_{\ell N}$ or large Yukawa coupling Y_S , see Fig. 19 and Fig. 20. Of course, for large decay width and small mass-splitting, the quantity x is small and hence $R_{\ell\ell}$ is small. However the decay width can be small for small mixing $V_{\ell N}$, (at least when $M_N < m_{H^\pm, H/A}$), comparable or even smaller than the mass splitting ΔM , so that x becomes large and $R_{\ell\ell}$ becomes close to 1. This is precisely what is shown in the right panel of Fig. 30. Assuming a light neutrino mass $m_\nu \sim 0.1$ eV we show the value of the mixing parameter $|V_{\ell N}|^2$ and mass M_N required to achieve LNV to LNC ratio $R_{\ell\ell} \geq 1/3$. We use the criterion $R_{\ell\ell} = 1/3$ ($\Delta M \approx \Gamma_N$) to distinguish between suppressed and unsuppressed LNV rates. For smaller light-neutrino-mass values the required value of the mixing angle $|V_{\ell N}|$ will be even smaller for a given mass M_N . Note that, although the mixing angle required to achieve maximum $R_{\ell\ell}$ is relatively small, the decay width is large enough to have heavy-neutrino decays inside the detector.

All in all, the above discussion shows that within our linear seesaw setup there is a wide parameter region with $\Delta M \approx \Gamma_N$, so that the ratio $R_{\ell\ell}$ can have any value within the range $[0, 1]$. This indicates the intrinsic presence of detectable lepton number violation rates at colliders, suggesting the that they may play a complementary role in probing the Majorana nature of neutrinos.

2. A generalized scheme

So far we have always assumed a genuine linear seesaw scenario where the heavy neutral leptons form quasi-Dirac pairs. Another way to achieve a large $R_{\ell\ell} \approx 1$ is to consider a generalized scheme containing a large Majorana mass entry breaking lepton number by two units and characterized by a large violation scale. Indeed, we can introduce such a $\Delta L = 2$ term M for the right-handed neutrinos ν^c , in co-existence with the $\Delta L = 1$ linear seesaw terms in Eq. 2, that break lepton number by one unit, i.e.

$$-\mathcal{L}_{\text{Yuk}} = Y_\nu^{ij} L_i^T C \nu_j^c \Phi + M_R^{ij} \nu_i^c C S_j + M^{ij} \nu_i^c C \nu_j^c + Y_S^{ij} L_i^T C S_j \chi_L + \text{h.c.} \quad (\text{B2})$$

The resulting neutral lepton mass matrix in the basis (ν_L, ν^c, S) is given as

$$\mathcal{M}_\nu = \begin{pmatrix} 0 & m_D & M_L \\ m_D^T & M & M_R \\ M_L^T & M_R^T & 0 \end{pmatrix}. \quad (\text{B3})$$

Under the assumption $M > M_R \gg m_D \gg M_L$ we integrate out the heavy fields ν^c and S and obtain the complete diagonalization of the extended seesaw mechanism. This results in the following physical masses for the neutral leptons,

$$m_\nu \approx m_D(M_L M_R^{-1})^T + (M_L M_R^{-1})m_D^T - (M_L M_R^{-1})M(M_L M_R^{-1})^T \quad (\text{B4})$$

$$M_{\nu^c} = \frac{1}{2} \left(M + \sqrt{M^2 + 4M_R^2} \right) \text{ and } M_S = \frac{1}{2} \left(M - \sqrt{M^2 + 4M_R^2} \right). \quad (\text{B5})$$

One sees that the light neutrinos acquire mass from the same source $M_L \sim v_\chi$ but now there is a quadratic term in addition to those characteristic of the linear seesaw mechanism. This new term is reminiscent from the conventional $\Delta L = 2$ seesaw mechanism. It is clear from the above mass matrices that the mass splitting of the heavy neutral leptons is now large, so they are closer to being pure Majorana. Thus, the addition of the large Majorana mass term for the singlet lepton ν^c makes it easier to induce large values for the ratio $R_{\ell\ell}$ characterizing LNV processes.

Appendix C: Other collider signatures

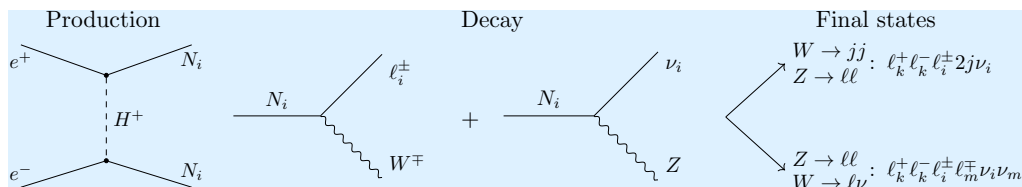


FIG. 31: Illustrative heavy-neutrino pair production and their decays via the charged and neutral currents for the case of $M_{N_i} < m_{H^\pm}$.

Our study can be expanded to include also the case where heavy neutrino mediators decay through the neutral current interaction. In Figs. 31, 32 and 33, we show possible final states that result when all heavy neutrinos decay through the neutral current, such as $N \rightarrow \nu Z$, or when one of them decays as $N \rightarrow \ell W$ and other one decay as $N \rightarrow \nu Z$. We have assumed the leptonic mode of the Z boson and leptonic/hadronic decay mode of the

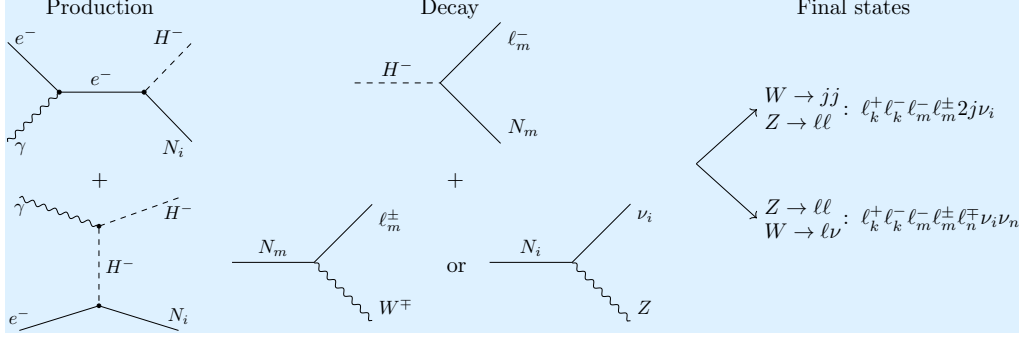


FIG. 32: Illustrative SM final states arising from the decay of the heavy neutrinos via the charged and neutral currents after being produced in association with charged Higgs, for the case of $M_{N_i} < m_{H^\pm}$.

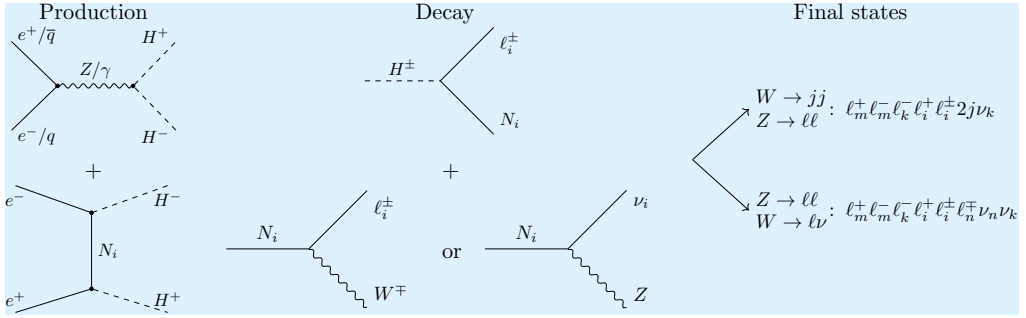


FIG. 33: Illustrative SM final states arising from the decay of the heavy neutrinos via the charged and neutral currents after being produced as the decay products of charged Higgs, for the case of $M_{N_i} < m_{H^\pm}$.

W boson.

-
- [1] T. Kajita, “Nobel Lecture: Discovery of atmospheric neutrino oscillations,” *Rev.Mod.Phys.* **88** (2016) 030501.
- [2] A. B. McDonald, “Nobel Lecture: The Sudbury Neutrino Observatory: Observation of flavor change for solar neutrinos,” *Rev.Mod.Phys.* **88** (2016) 030502.
- [3] **KamLAND** Collaboration, K. Eguchi *et al.*, “First results from KamLAND: Evidence for reactor anti-neutrino disappearance,” *Phys.Rev.Lett.* **90** (2003) 021802, [arXiv:hep-ex/0212021 \[hep-ex\]](#).
- [4] **K2K** Collaboration, M. Ahn *et al.*, “Indications of neutrino oscillation in a 250 km long baseline experiment,” *Phys.Rev.Lett.* **90** (2003) 041801, [arXiv:hep-ex/0212007 \[hep-ex\]](#).
- [5] S. Weinberg, “Varieties of Baryon and Lepton Nonconservation,” *Phys.Rev.D* **22** (1980) 1694.
- [6] J. Schechter and J. W. F. Valle, “Neutrino Masses in $SU(2) \times U(1)$ Theories,” *Phys.Rev.D*

- 22** (1980) 2227.
- [7] R. Mohapatra and J. W. F. Valle, “Neutrino Mass and Baryon Number Nonconservation in Superstring Models,” vol. 34, p. 1642. 1986.
- [8] M. Gonzalez-Garcia and J. W. F. Valle, “Fast Decaying Neutrinos and Observable Flavor Violation in a New Class of Majoron Models,” *Phys.Lett.B* **216** (1989) 360–366.
- [9] E. K. Akhmedov *et al.*, “Left-right symmetry breaking in NJL approach,” *Phys.Lett.B* **368** (1996) 270–280, [arXiv:hep-ph/9507275 \[hep-ph\]](#).
- [10] E. K. Akhmedov *et al.*, “Dynamical left-right symmetry breaking,” *Phys.Rev.D* **53** (1996) 2752–2780, [arXiv:hep-ph/9509255 \[hep-ph\]](#).
- [11] M. Malinsky, J. Romao, and J. W. F. Valle, “Novel supersymmetric SO(10) seesaw mechanism,” *Phys.Rev.Lett.* **95** (2005) 161801, [arXiv:hep-ph/0506296 \[hep-ph\]](#).
- [12] J. Schechter and J. W. F. Valle, “Neutrino Decay and Spontaneous Violation of Lepton Number,” *Phys.Rev.D* **25** (1982) 774.
- [13] M. Dittmar, A. Santamaria, M. Gonzalez-Garcia, and J. W. F. Valle, “Production Mechanisms and Signatures of Isosinglet Neutral Heavy Leptons in Z^0 Decays,” *Nucl.Phys.B* **332** (1990) 1–19.
- [14] M. Gonzalez-Garcia, A. Santamaria, and J. W. F. Valle, “Isosinglet Neutral Heavy Lepton Production in Z Decays and Neutrino Mass,” *Nucl.Phys.B* **342** (1990) 108–126.
- [15] Aguilar-Saavedra *et al.*, “Flavour in heavy neutrino searches at the LHC,” *Phys.Rev.D* **85** (2012) 091301, [arXiv:1203.5998 \[hep-ph\]](#).
- [16] S. Das, F. Deppisch, O. Kittel, and J. W. F. Valle, “Heavy Neutrinos and Lepton Flavour Violation in Left-Right Symmetric Models at the LHC,” *Phys.Rev.D* **86** (2012) 055006, [arXiv:1206.0256 \[hep-ph\]](#).
- [17] F. F. Deppisch, N. Desai, and J. W. F. Valle, “Is charged lepton flavor violation a high energy phenomenon?,” *Phys.Rev.D* **89** (2014) 051302, [arXiv:1308.6789 \[hep-ph\]](#).
- [18] M. Drewes and J. Hajer, “Heavy Neutrinos in displaced vertex searches at the LHC and HL-LHC,” *JHEP* **02** (2020) 070, [arXiv:1903.06100 \[hep-ph\]](#).
- [19] G. Cottin *et al.*, “Long-lived heavy neutral leptons with a displaced shower signature at CMS,” *JHEP* **02** (2023) 011, [arXiv:2210.17446 \[hep-ph\]](#).
- [20] ATLAS Collaboration, G. Aad *et al.*, “Search for heavy neutral leptons in decays of W bosons produced in 13 TeV pp collisions using prompt and displaced signatures with the ATLAS detector,” *JHEP* **10** (2019) 265, [arXiv:1905.09787 \[hep-ex\]](#).
- [21] CMS Collaboration, A. M. Sirunyan *et al.*, “Search for heavy neutral leptons in events with three charged leptons in proton-proton collisions at $\sqrt{s} = 13$ TeV,” *Phys.Rev.Lett.* **120** (2018) 221801, [arXiv:1802.02965 \[hep-ex\]](#).
- [22] CMS Collaboration, A. Tumasyan *et al.*, “Inclusive nonresonant multilepton probes of new phenomena at $s=13$ TeV,” *Phys.Rev.D* **105** no. 11, (2022) 112007, [arXiv:2202.08676](#)

- [hep-ex].
- [23] FCC Collaboration, A. Abada *et al.*, “FCC-ee: The Lepton Collider,” *Eur.Phys.J.ST* **228** no. 2, (2019) 261–623.
- [24] FCC Collaboration, A. Abada *et al.*, “FCC Physics Opportunities,” *Eur.Phys.J.C* **79** no. 6, (2019) 474.
- [25] J. L. Feng *et al.*, “The Forward Physics Facility at the High-Luminosity LHC,” 3, 2022. [arXiv:2203.05090 \[hep-ex\]](#).
- [26] J. Bernabeu *et al.*, “Lepton Flavor Nonconservation at High-Energies in a Superstring Inspired Standard Model,” *Phys.Lett.B* **187** (1987) 303–308.
- [27] P. Langacker and D. London, “Lepton Number Violation and Massless Nonorthogonal Neutrinos,” *Phys.Rev.D* **38** (1988) 907.
- [28] G. Branco, M. Rebelo, and J. W. F. Valle, “Leptonic CP Violation With Massless Neutrinos,” *Phys.Lett.B* **225** (1989) 385–392.
- [29] N. Rius and J. W. F. Valle, “Leptonic CP Violating Asymmetries in Z^0 Decays,” *Phys.Lett.B* **246** (1990) 249–255.
- [30] M. Gonzalez-Garcia and J. W. F. Valle, “Enhanced lepton flavor violation with massless neutrinos: A Study of muon and tau decays,” *Mod.Phys.Lett.A* **7** (1992) 477–488.
- [31] F. Deppisch and J. W. F. Valle, “Enhanced lepton flavor violation in the supersymmetric inverse seesaw model,” *Phys.Rev.D* **72** (2005) 036001, [arXiv:hep-ph/0406040 \[hep-ph\]](#).
- [32] F. Deppisch, T. Kosmas, and J. W. F. Valle, “Enhanced μ - e conversion in nuclei in the inverse seesaw model,” *Nucl.Phys.B* **752** (2006) 80–92, [arXiv:hep-ph/0512360 \[hep-ph\]](#).
- [33] A. Ilakovac and A. Pilaftsis, “Flavor violating charged lepton decays in seesaw-type models,” *Nucl.Phys.B* **437** (1995) 491, [arXiv:hep-ph/9403398 \[hep-ph\]](#).
- [34] E. Arganda, M. Herrero, and A. Teixeira, “ μ - e conversion in nuclei within the CMSSM seesaw: Universality versus non-universality,” *JHEP* **10** (2007) 104, [arXiv:0707.2955 \[hep-ph\]](#).
- [35] A. Abada, V. De Romeri, S. Monteil, J. Orloff, and A. Teixeira, “Indirect searches for sterile neutrinos at a high-luminosity Z-factory,” *JHEP* **04** (2015) 051, [arXiv:1412.6322 \[hep-ph\]](#).
- [36] A. Abada, V. De Romeri, and A. Teixeira, “Impact of sterile neutrinos on nuclear-assisted cLFV processes,” *JHEP* **02** (2016) 083, [arXiv:1510.06657 \[hep-ph\]](#).
- [37] S. M. Boucenna, S. Morisi, and J. W. F. Valle, “The low-scale approach to neutrino masses,” *Adv.High Energy Phys.* **2014** (2014) 831598, [arXiv:1404.3751 \[hep-ph\]](#).
- [38] D. Fontes, J. C. Romao, and J. W. F. Valle, “Electroweak Breaking and Higgs Boson Profile in the Simplest Linear Seesaw Model,” *JHEP* **10** (2019) 245, [arXiv:1908.09587 \[hep-ph\]](#).
- [39] G. Branco *et al.*, “Theory and phenomenology of two-Higgs-doublet models,” *Phys.Rept.* **516** (2012) 1–102, [arXiv:1106.0034 \[hep-ph\]](#).

- [40] G. Bhattacharyya and D. Das, “Scalar sector of two-Higgs-doublet models: A minireview,” *Pramana* **87** no. 3, (2016) 40, [arXiv:1507.06424 \[hep-ph\]](#).
- [41] L. Wang, J. M. Yang, and Y. Zhang, “Two-Higgs-doublet models in light of current experiments: a brief review,” [arXiv:2203.07244 \[hep-ph\]](#).
- [42] D. Eriksson, J. Rathsmann, and O. Stal, “2HDMC: Two-Higgs-Doublet Model Calculator Physics and Manual,” *Comput.Phys.Commun.* **181** (2010) 189–205, [arXiv:0902.0851 \[hep-ph\]](#).
- [43] **MEG** Collaboration, J. Adam *et al.*, “New constraint on the existence of the $\mu^+ \rightarrow e^+ \gamma$ decay,” *Phys.Rev.Lett.* **110** (2013) 201801, [arXiv:1303.0754 \[hep-ex\]](#).
- [44] T. Barklow *et al.*, “ILC Operating Scenarios,” [arXiv:1506.07830 \[hep-ex\]](#).
- [45] **CLICdp**, **CLIC** Collaboration, P. Burrows *et al.*, “The Compact Linear Collider (CLIC) - 2018 Summary Report,” *CERN Yellow Rep.Monogr.* **2** (2018) , [arXiv:1812.06018 \[physics.acc-ph\]](#).
- [46] **CEPC Study Group** Collaboration, J. B. Guimarães da Costa *et al.*, “CEPC Conceptual Design Report: Volume 2 - Physics & Detector,” [arXiv:1811.10545 \[hep-ex\]](#).
- [47] V. I. Telnov, “Status of gamma gamma, gamma electron colliders,” vol. 82, pp. 359–366. 2000. [arXiv:hep-ex/9908005 \[hep-ex\]](#).
- [48] F. Bechtel *et al.*, “Studies for a photon collider at the ILC,” *Nucl.Instrum.Meth.A* **564** (2006) 243–261, [arXiv:physics/0601204 \[physics\]](#).
- [49] I. Ginzburg, G. Kotkin, S. Panfil, and V. Serbo, “The W^\pm Boson Production on the Colliding e^+e^- , γe and $\gamma\gamma$ Beams,” *Nucl.Phys.B* **228** (1983) 285–300. [Erratum: *Nucl.Phys.B* 243, 550–550 (1984)].
- [50] I. Ginzburg, G. Kotkin, S. Panfil, V. Serbo, and V. I. Telnov, “Colliding gamma e and gamma gamma Beams Based on the Single Pass $e^+ e^-$ Accelerators. 2. Polarization Effects. Monochromatization Improvement,” vol. 219, pp. 5–24. 1984.
- [51] M. M. Velasco *et al.*, “Photon Photon and Electron Photon Colliders with Energies Below a TeV,” vol. C010630, p. E3005. 2001. [arXiv:hep-ex/0111055 \[hep-ex\]](#).
- [52] V. I. Telnov, “Problems of Obtaining $\gamma\gamma$ and γe Colliding Beams at Linear Colliders,” *Nucl.Instrum.Meth.A* **294** (1990) 72–92.
- [53] A. S. Joshipura and J. W. F. Valle, “Invisible Higgs decays and neutrino physics,” *Nucl.Phys.B* **397** (1993) 105–122.
- [54] J. W. F. Valle, “Neutrinoless Double Beta Decay With Quasi Dirac Neutrinos,” *Phys.Rev.D* **27** (1983) 1672–1674.
- [55] G. Anamiati, M. Hirsch, and E. Nardi, “Quasi-Dirac neutrinos at the LHC,” *JHEP* **10** (2016) 010, [arXiv:1607.05641 \[hep-ph\]](#).
- [56] **ATLAS** Collaboration, G. Aad *et al.*, “Observation of a new particle in the search for the Standard Model Higgs boson with the ATLAS detector at the LHC,” *Phys.Lett.B* **716**

- (2012) 1–29, [arXiv:1207.7214 \[hep-ex\]](#).
- [57] **CMS** Collaboration, S. Chatrchyan *et al.*, “Observation of a New Boson at a Mass of 125 GeV with the CMS Experiment at the LHC,” *Phys.Lett.B* **716** (2012) 30–61, [arXiv:1207.7235 \[hep-ex\]](#).
- [58] **Particle Data Group** Collaboration, P. Zyla *et al.*, “Review of Particle Physics,” *PTEP* **2020** (2020) 083C01.
- [59] M. E. Peskin and T. Takeuchi, “Estimation of oblique electroweak corrections,” *Phys.Rev.D* **46** (1992) 381–409.
- [60] A. Batra, P. Bharadwaj, S. Mandal, R. Srivastava, and J. W. F. Valle, “W-mass anomaly in the simplest linear seesaw mechanism,” *Phys.Lett.B* **834** (2022) 137408, [arXiv:2208.04983 \[hep-ph\]](#).
- [61] **CDF** Collaboration, T. Aaltonen *et al.*, “High-precision measurement of the W boson mass with the CDF II detector,” *Science* **376** no. 6589, (2022) abk1781.
- [62] C.-T. Lu, L. Wu, Y. Wu, and B. Zhu, “Electroweak precision fit and new physics in light of the W boson mass,” *Phys. Rev. D* **106** no. 3, (2022) 035034, [arXiv:2204.03796 \[hep-ph\]](#).
- [63] S. Glashow, J. Iliopoulos, and L. Maiani, “Weak Interactions with Lepton-Hadron Symmetry,” *Phys.Rev.D* **2** (1970) 1285–1292.
- [64] D. Forero, S. Morisi, M. Tortola, and J. W. F. Valle, “Lepton flavor violation and non-unitary lepton mixing in low-scale type-I seesaw,” *JHEP* **09** (2011) 142, [arXiv:1107.6009 \[hep-ph\]](#).
- [65] P. Minkowski, “ $\mu \rightarrow e\gamma$ at a Rate of One Out of 10^9 Muon Decays?,” *Phys.Lett.B* **67** (1977) 421–428.
- [66] W. Marciano and A. Sanda, “Exotic Decays of the Muon and Heavy Leptons in Gauge Theories,” *Phys.Lett.B* **67** (1977) 303–305.
- [67] T. Cheng and L.-F. Li, “ $\mu \rightarrow e\gamma$ in Theories With Dirac and Majorana Neutrino Mass Terms,” *Phys.Rev.Lett.* **45** (1980) 1908.
- [68] C. Lim and T. Inami, “Lepton Flavor Nonconservation and the Mass Generation Mechanism for Neutrinos,” *Prog.Theor.Phys.* **67** (1982) 1569.
- [69] J. Casas and A. Ibarra, “Oscillating neutrinos and $\mu \rightarrow e, \gamma$,” *Nucl.Phys.B* **618** (2001) 171–204, [arXiv:hep-ph/0103065 \[hep-ph\]](#).
- [70] I. Cordero-Carrión, M. Hirsch, and A. Vicente, “Master Majorana neutrino mass parametrization,” *Phys.Rev.D* **99** no. 7, (2019) 075019, [arXiv:1812.03896 \[hep-ph\]](#).
- [71] I. Cordero-Carrión, M. Hirsch, and A. Vicente, “General parametrization of Majorana neutrino mass models,” *Phys.Rev.D* **101** no. 7, (2020) 075032, [arXiv:1912.08858 \[hep-ph\]](#).
- [72] P. de Salas *et al.*, “2020 global reassessment of the neutrino oscillation picture,” *JHEP* **02** (2021) 071, [arXiv:2006.11237 \[hep-ph\]](#).

- [73] L. Lavoura, “General formulae for $f(1) \rightarrow f(2) \gamma$,” *Eur.Phys.J.C* **29** (2003) 191–195, [arXiv:hep-ph/0302221 \[hep-ph\]](#).
- [74] J. Schechter and J. W. F. Valle, “Neutrinoless Double beta Decay in $SU(2) \times U(1)$ Theories,” *Phys.Rev.D* **25** (1982) 2951.
- [75] A. Batra, P. Bharadwaj, S. Mandal, R. Srivastava, and J. W. F. Valle, “Heavy neutrino signatures from leptophilic Higgs portal in the linear seesaw,” [arXiv:2304.06080 \[hep-ph\]](#).
- [76] **ATLAS** Collaboration, M. Aaboud *et al.*, “Search for additional heavy neutral Higgs and gauge bosons in the ditau final state produced in 36 fb^{-1} of pp collisions at $\sqrt{s} = 13 \text{ TeV}$ with the ATLAS detector,” *JHEP* **01** (2018) 055, [arXiv:1709.07242 \[hep-ex\]](#).
- [77] **ATLAS** Collaboration, G. Aad *et al.*, “Search for heavy Higgs bosons decaying into two tau leptons with the ATLAS detector using pp collisions at $\sqrt{s} = 13 \text{ TeV}$,” *Phys.Rev.Lett.* **125** no. 5, (2020) 051801, [arXiv:2002.12223 \[hep-ex\]](#).
- [78] **CMS** Collaboration, V. Khachatryan *et al.*, “Search for a charged Higgs boson in pp collisions at $\sqrt{s} = 8 \text{ TeV}$,” *JHEP* **11** (2015) 018, [arXiv:1508.07774 \[hep-ex\]](#).
- [79] **ATLAS** Collaboration, M. Aaboud *et al.*, “Search for charged Higgs bosons decaying via $H^\pm \rightarrow \tau^\pm \nu_\tau$ in the τ +jets and τ +lepton final states with 36 fb^{-1} of pp collision data recorded at $\sqrt{s} = 13 \text{ TeV}$ with the ATLAS experiment,” *JHEP* **09** (2018) 139, [arXiv:1807.07915 \[hep-ex\]](#).
- [80] **ATLAS** Collaboration, M. Aaboud *et al.*, “Search for charged Higgs bosons decaying into top and bottom quarks at $\sqrt{s} = 13 \text{ TeV}$ with the ATLAS detector,” *JHEP* **11** (2018) 085, [arXiv:1808.03599 \[hep-ex\]](#).
- [81] **ALEPH, DELPHI, L3, OPAL, LEP** Collaboration, G. Abbiendi *et al.*, “Search for Charged Higgs bosons: Combined Results Using LEP Data,” *Eur.Phys.J.C* **73** (2013) 2463, [arXiv:1301.6065 \[hep-ex\]](#).
- [82] Q.-H. Cao, E. Ma, and G. Rajasekaran, “Observing the Dark Scalar Doublet and its Impact on the Standard-Model Higgs Boson at Colliders,” *Phys.Rev.D* **76** (2007) 095011, [arXiv:0708.2939 \[hep-ph\]](#).
- [83] M. Gustafsson, E. Lundstrom, L. Bergstrom, and J. Edsjo, “Significant Gamma Lines from Inert Higgs Dark Matter,” *Phys.Rev.Lett.* **99** (2007) 041301, [arXiv:astro-ph/0703512 \[astro-ph\]](#).
- [84] P. Posch, “Enhancement of $h \rightarrow \gamma \gamma$ in the Two Higgs Doublet Model Type I,” *Phys.Lett.B* **696** (2011) 447–453, [arXiv:1001.1759 \[hep-ph\]](#).
- [85] A. Batra, S. Mandal, and R. Srivastava, “ $h \rightarrow \Upsilon \gamma$ Decay: Smoking Gun Signature of Wrong-Sign $hb\bar{b}$ Coupling,” [arXiv:2209.01200 \[hep-ph\]](#).
- [86] **ATLAS, CMS** Collaboration, G. Aad *et al.*, “Measurements of the Higgs boson production and decay rates and constraints on its couplings from a combined ATLAS and

- CMS analysis of the LHC pp collision data at $\sqrt{s} = 7$ and 8 TeV,” *JHEP* **08** (2016) 045, [arXiv:1606.02266 \[hep-ex\]](#).
- [87] **ATLAS** Collaboration, G. Aad *et al.*, “Combined measurements of Higgs boson production and decay using up to 80 fb⁻¹ of proton-proton collision data at $\sqrt{s} = 13$ TeV collected with the ATLAS experiment,” *Phys.Rev.D* **101** (2020) 012002, [arXiv:1909.02845 \[hep-ex\]](#).
- [88] **ATLAS** Collaboration, “Measurement of the properties of Higgs boson production at $\sqrt{s} = 13$ TeV in the $H \rightarrow \gamma\gamma$ channel using 139 fb⁻¹ of pp collision data with the ATLAS experiment,” [arXiv:2207.00348 \[hep-ex\]](#).
- [89] A. Atre, T. Han, S. Pascoli, and B. Zhang, “The Search for Heavy Majorana Neutrinos,” *JHEP* **05** (2009) 030, [arXiv:0901.3589 \[hep-ph\]](#).
- [90] S. Banerjee, P. S. B. Dev, A. Ibarra, T. Mandal, and M. Mitra, “Prospects of Heavy Neutrino Searches at Future Lepton Colliders,” *Phys. Rev. D* **92** (2015) 075002, [arXiv:1503.05491 \[hep-ph\]](#).
- [91] A. Das, Y. Gao, and T. Kamon, “Heavy neutrino search via semileptonic Higgs decay at the LHC,” *Eur. Phys. J. C* **79** no. 5, (2019) 424, [arXiv:1704.00881 \[hep-ph\]](#).
- [92] A. Das, S. Jana, S. Mandal, and S. Nandi, “Probing right handed neutrinos at the LHeC and lepton colliders using fat jet signatures,” *Phys. Rev. D* **99** no. 5, (2019) 055030, [arXiv:1811.04291 \[hep-ph\]](#).
- [93] M. Drewes, “Distinguishing Dirac and Majorana Heavy Neutrinos at Lepton Colliders,” vol. ICHEP2022, p. 608. 2022. [arXiv:2210.17110 \[hep-ph\]](#).
- [94] K. Mekała, J. Reuter, and A. F. Żarnecki, “Heavy neutrinos at future linear e^+e^- colliders,” *JHEP* **06** (2022) 010, [arXiv:2202.06703 \[hep-ph\]](#).
- [95] A. Das, S. Mandal, and S. Shil, “Testing electroweak scale seesaw models at $e^- \gamma$ and $\gamma\gamma$ colliders,” [arXiv:2304.06298 \[hep-ph\]](#).
- [96] A. M. Abdullahi *et al.*, “The Present and Future Status of Heavy Neutral Leptons,” in *2022 Snowmass Summer Study*. 3, 2022. [arXiv:2203.08039 \[hep-ph\]](#).
- [97] E. J. Chun, A. Das, S. Mandal, M. Mitra, and N. Sinha, “Sensitivity of Lepton Number Violating Meson Decays in Different Experiments,” *Phys.Rev.D* **100** no. 9, (2019) 095022, [arXiv:1908.09562 \[hep-ph\]](#).
- [98] F. del Aguila, J. de Blas, and M. Perez-Victoria, “Effects of new leptons in Electroweak Precision Data,” *Phys.Rev.D* **78** (2008) 013010, [arXiv:0803.4008 \[hep-ph\]](#).
- [99] S. Antusch and O. Fischer, “Testing sterile neutrino extensions of the Standard Model at future lepton colliders,” *JHEP* **05** (2015) 053, [arXiv:1502.05915 \[hep-ph\]](#).
- [100] P. Li, Z. Liu, and K.-F. Lyu, “Heavy neutral leptons at muon colliders,” *JHEP* **03** (2023) 231, [arXiv:2301.07117 \[hep-ph\]](#).
- [101] J. P. Delahaye, M. Diemoz, K. Long, B. Mansoulié, N. Pastrone, L. Rivkin, D. Schulte, A. Skrinsky, and A. Wulzer, “Muon Colliders,” [arXiv:1901.06150 \[physics.acc-ph\]](#).

- [102] S. Antusch, J. Hajer, and J. Roskopp, “Simulating lepton number violation induced by heavy neutrino-antineutrino oscillations at colliders,” [arXiv:2210.10738 \[hep-ph\]](#).
- [103] S. Antusch and J. Roskopp, “Heavy Neutrino-Antineutrino Oscillations in Quantum Field Theory,” *JHEP* **03** (2021) 170, [arXiv:2012.05763 \[hep-ph\]](#).